PERGAMON

Deep-Sea Research II 49 (2002) 2443–2469

DEEP-SEA RESEARCH
PART II

www.elsevier.com/locate/dsr2

Seasonal and interannual variability of CO_2 in the equatorial Pacific

Richard A. Feely[a,*], Jacqueline Boutin[b], Catherine E. Cosca[a], Yves Dandonneau[b], Jacqueline Etcheto[b], Hisayuki Y. Inoue[c], Masao Ishii[c], Corinne Le Quéré[d], Denis J. Mackey[e], Michael McPhaden[a], Nicolas Metzl[f], Alain Poisson[f], Rik Wanninkhof[g]

[a] *Pacific Marine Environmental Laboratory, National Oceanic and Atmospheric Administration, 7600 Sand Point Way N.E., Seattle, WA 98115-0070, USA*

[b] *LODYC, UMR 7617 CNRS/IRD, Universite Pierre et Marie Curie, Paris, France*

[c] *Geochemical Research Department, Meteorological Research Institute, Nagamine 1-1, Tsukuba, Ibaraki, 305-0052, Japan*

[d] *Max-Planck-Institut fuer Biogeochemie, Carl-Zeiss-Promenade 10, 07745 Jena, Germany*

[e] *CSIRO Marine Research, PO Box 1538, Hobart, Tasmania, 7001 Australia*

[f] *Laboratoire de Physique et Chimie Marines/CNRS, IPSL, Université Pierre et Marie Curie, 4 place Jussieu, 75252 Paris cedex 05 France*

[g] *Atlantic Oceanographic and Meteorological Laboratory, NOAA, 4301 Rickenbacker Causeway, Miami, FL 33149, USA*

Received 19 June 2000; received in revised form 5 October 2001; accepted 3 November 2001

Abstract

As part of the JGOFS field program, extensive CO_2 partial-pressure measurements were made in the atmosphere and in the surface waters of the equatorial Pacific from 1992 to 1999. For the first time, we are able to determine how processes occurring in the western portion of the equatorial Pacific impact the sea–air fluxes of CO_2 in the central and eastern regions. These 8 years of data are compared with the decade of the 1980s. Over this period, surface-water pCO_2 data indicate significant seasonal and interannual variations. The largest decreases in fluxes were associated with the 1991–94 and 1997–98 El Niño events. The lower sea–air CO_2 fluxes during these two El Niño periods were the result of the combined effects of interconnected large-scale and locally forced physical processes: (1) development of a low-salinity surface cap as part of the formation of the warm pool in the western and central equatorial Pacific, (2) deepening of the thermocline by propagating Kelvin waves in the eastern Pacific, and (3) the weakening of the winds in the eastern half of the basin. These processes serve to reduce pCO_2 values in the central and eastern equatorial Pacific towards near-equilibrium values at the height of the warm phase of ENSO. In the western equatorial Pacific there is a small but significant increase in seawater pCO_2 during strong El Niño events (i.e., 1982–83 and 1997–98) and little or no change during weak El Niño events (1991–94). The net effect of these interannual variations is a lower-than-normal CO_2 flux to the atmosphere from the equatorial Pacific during El Niño. The annual average fluxes indicate that during strong El Niños the release to the atmosphere is 0.2–0.4 Pg C yr^{-1} compared to 0.8–1.0 Pg C yr^{-1} during non-El Niño years.

*Corresponding author. Tel.: +1-206-526-6214; fax: +1-206-526-6744.
E-mail address: feely@pmel.noaa.gov (R.A. Feely).

0967-0645/02/$ - see front matter © 2002 Published by Elsevier Science Ltd.
PII: S0967-0645(02)00044-9

1. Introduction

The equatorial ocean plays an important role in the global carbon cycle. Upwelling in the oceanic equatorial belt annually supplies approximately 0.6–1.5 Pg C as CO_2 to the atmosphere with most of the release occurring in the equatorial Pacific (Smethie et al., 1985; Tans et al., 1990; Feely et al., 1997; Takahashi et al., 1997). During non-El Niño years, waters enriched in CO_2 extend from the coastal waters west of South America to approximately 160°E (Cosca et al., 2002). The large area affected by the upwelling process makes this region the largest oceanic source of CO_2 to the atmosphere. Physical processes and biological productivity controls the strength of this source from year to year (Feely et al., 1997, 1999a, b; Chavez et al., 1999). During the 1990s, the international Joint Global Ocean Flux Study (JGOFS) supported research directed towards a quantitative understanding of the carbon budget in the equatorial Pacific. A comprehensive set of atmospheric and surface ocean measurements of carbon dioxide partial pressure (pCO_2) and supporting hydrographic data were obtained from 1990 through 1999 (Table 1). The 1992–94 cruises occurred during a prolonged mild El Niño, the 1995–96 cruises occurred during weak La Niña conditions (Feely et al., 1999a, b), and the 1997–98 cruises occurred during the strongest El Niño of this century. Many of the previous modeling and field studies of seawater pCO_2 (pCO_{2sw}) in this region have emphasized the different time scales of variability in the equatorial Pacific (Keeling and Revelle, 1985; Feely et al., 1987, 1994, 1995, 1997; Inoue and Sugimura, 1992; Inoue, 2000; Inoue et al., 1995, 1996, 2001; Wong et al., 1993; Goyet and Peltzer, 1994; Winguth et al., 1994; Dandonneau, 1995; Meyers and O'Brien, 1995; Murphy et al., 1995; Archer et al., 1996; Wanninkhof et al., 1995, 1996; Takahashi et al., 1997; Boutin et al., 1999; Etcheto et al., 1999). However, few studies have attempted to link the simultaneous changes occurring in the eastern and western parts of the equatorial Pacific (Boutin et al., 1999). In this synthesis, we summarize the research on the air–sea exchange of CO_2 in the equatorial Pacific with an emphasis on how processes occurring in the western side of the region directly affect the eastern side, and how these processes affect the annual flux of CO_2 from the entire region.

1.1. Circulation processes

The horizontal and vertical circulation patterns in the equatorial Pacific exert a dominant control on the overall trends of surface water pCO_2. The region is defined here as spanning from 10°N–10°S, and from the coast of South America (80°W) to New Guinea (135°E). Spatially, the equatorial Pacific can be divided into two major regions that have different pCO_2 dynamics: the High Nutrient Low Chlorophyll (HNLC) region from the coast of South America to the eastern edge of the warm pool, nominally at approximately 160°E; and the western Pacific warm pool, which nominally extends from about 135°E to 160°E under normal conditions but moves eastward in response to El Niño. During normal or "cold conditions" the trade winds drive upwelling along the equator. The source of this upwelled water is the narrow Equatorial Undercurrent (EUC), which flows eastward across the basin (Toggweiler and Carson, 1995). The upwelling results in a cold tongue along the equator from the coast of South America to about 160°E during normal conditions. Every 3–7 years the central and eastern equatorial Pacific warms dramatically as El Niño develops. The recent 1997–98 El Niño was, by some measures, the strongest of the 20th century, with major impacts on global weather patterns (McPhaden, 1999).

During El Niño events, the easterly trade winds in the western and central equatorial Pacific weaken and reverse (Fig. 1), a process punctuated by episodic westerly wind events of 1–3 weeks duration. Westerly winds accelerate surface currents which advect the western Pacific warm pool (with surface water temperatures greater than about 28.5°C) eastward along the equator. These westerly episodes are often the manifestation of the Madden and Julian Oscillation (MJO), a 30–60 day wave-like disturbance in the atmosphere originating over the Indian Ocean. They also can be related to generic westerly wind bursts (e.g., Luther et al., 1983), cold air outbreaks from higher

Table 1
Cruise data sets used in this synthesis

Organization	Cruise name	Cruise dates	Latitude	Longitude
CSIRO, Australia	FR08/90	October 2–October 17, 1990	1°S–5°N	147°E
			10°S–5°N	155°E
	FR05/92	June 15–July 13, 1992	1.5°S–6°N	147°E
			10°S–10°N	155°E
	FR08/93	November 5–December 1, 1993	10°S–10°N	155°E
LPCM/CNRS, France	FLUPAC	September 26–October 30, 1994	11°S–6°N	165°E
	FLUPAC		0°	166°E–150°W
	FLUPAC		0°–18°S	150°W
	OLIPAC	November 5–29, 1994	11°N–16°S	150°W
LODYC/UMR, France	ALIZE II	January 3–March 5, 1991	0°	100°W–165°E
	ECOA 1	August 9–21, 1991	8°N–20°S	100°W
	ECOA 2	November 5–15, 1991	8°N–20°S	100°W
	ECOA 3	February 29–March 10, 1992	8°N–20°S	100°W
	ECOA 4	June 16–27, 1992	8°N–20°S	100°W
	ECOA 5	September 22–October 5, 1992	8°N–20°S	100°W
	ECOA 9	January 13- 24, 1994	8°N–20°S	100°W
	ECOA 10	April 21–May 2, 1994	8°N–20°S	100°W
	ECOA 11	August 13–26, 1994	8°N–20°S	100°W
	ECOA 14	May 24–June 3, 1995	8°N–20°S	100°W
	ECOA 15	September 1–13, 1995	8°N–20°S	100°W
	ECOA 16	December 12–27, 1995	8°N–20°S	100°W
	ECOA 17	March 21–31, 1996	8°N–20°S	100°W
	ECOA 18	June 23–July 7, 1996	8°N–20°S	100°W
	ECOA 19	September 24–October 5, 1996	8°N–20°S	100°W
	ECOA 20	November 5–November 29, 1994	8°N–20°S	100°W
MRI/JMA, Japan	KH90-2	10 September–3 December, 1990	20°N–17°S	140°E–150°W
	KY9401	12 January–3 February, 1994	0°	138°E–165°W
	KY9406	20 November–13 December, 1994	0°	147°E–165°W
	KY9801	7–28 January, 1998	0°	138°E–165°W
	MR98-01	2–7 February, 1998	0°	180°E–163°W
	MR98-K02	3–16 January, 1999	0°	145°E–170°W
	RY8101	20–30 January, 1981	34°N–3°N	137°E
	RY8201	19–30 January, 1982	34°N–3°N	137°E
	RY8301	19–28 January, 1983	34°N–3°N	137°E
	RY8401	20–31 January, 1984	34°N–3°N	137°E
	RY8501	18–29 January, 1985	34°N–3°N	137°E
	RY8601	19–29 January, 1986	34°N–3°N	137°E
	RY8701	14–25 January, 1987	34°N–3°N	137°E
	RY8801	16–29 January, 1988	34°N–3°N	137°E
	RY8901	19–29 January, 1989	34°N–3°N	137°E
	RY9001	20 January–1 February, 1990	34°N–3°N	137°E
	RY9101	19–30 January, 1991	34°N–3°N	137°E
	RY9201	20 January–2 February, 1992	34°N–3°N	137°E
	RY9301	20 January–2 February, 1993	34°N–3°N	137°E
	RY9401	20–31 January, 1994	34°N–3°N	137°E
	RY9501	19 January–11 February, 1995	34°N–3°N	137°E
	RY9601	17 January–8 February , 1996	34°N–3°N	137°E
	RY9701	18 January–8 February, 1997	34°N–3°N	137°E

Table 1 (*continued*)

Organization	Cruise name	Cruise dates	Latitude	Longitude
AOML/NOAA, USA	EqPac Spring, 1992	March 2–March 14, 1992	10°N–8°S	110°W, 95°W
		April 4–April 13, 1992	10°N–10°S	170°W
		April 25–May 5, 1992	10°S–9°N	140°W
PMEL/NOAA, USA	EqPac Fall, 1992	August 20–August 25, 1992	8°N–8°S	170°W
		September 11–October 2, 1992	10°N–10°S	140°W, 125°W
		October 12–November 18, 1992	10°N–10°S	110°W
		November 19–December 8, 1992	2°N–10°S	95°W
PMEL/NOAA, USA	Discoverer TAO Cruise	March 3–March 14, 1993	2°N–10°S	170°W
AOML/NOAA, USA	EqPac Spring, 1993	February 28–March 13, 1993	8°N–8°S	95°W, 110°W
		April 23–April 28, 1993	6°N–5°S	140°W
		April 30–May 3, 1993	2°S–8°N	125°W
AOML/NOAA, USA	EqPac Spring, 1994	April 5–April 19, 1994	10°S–10°N	110°W
		April 19–April 22, 1994	5°N–5°S	95°W
		April 29–May 5, 1994	8°S–10°N	125°W
		May 22–May 29, 1994	10°N–9°S	140°W
		June 5–June 8, 1994	0°–5°N	110°W
AOML/NOAA, USA	EqPac Fall, 1994	August 6–August 13, 1994	8°N–8°S	95°W
		August 15–August 20, 1994	2°S–10°N	110°W
		September 3–September 12, 1994	10°N–8°S	125°W
		September 15–September 16, 1994	8°S–2°S	110°W
		November 2–November 19, 1994	10°N–8°S	170°W, 180°
AOML/NOAA, USA	EqPac Fall, 1995	November 30–December 14, 1994	8°N–8°S	170°W, 180°
		December 24–December 30, 1994	9°S–8°N	155°W
AOML/NOAA, USA	EpPac Spring, 1996	May 5–May 22, 1996	8°N–8°S	95°W, 110°W
		June 6–June 17, 1996	10°N–6°S	140°W
		June 17–June 30, 1996	6°S–4°N	125°W
PMEL/NOAA, USA	Ka'imimoana TAO cruises	June 26–July 3, 1996	8°N–8°S	180°
	1996	July 25–August 1, 1996	5°N–5°S	170°W
		August 6–August 11, 1996	8°S–8°N	155°W
		August 31–September 6, 1996	5°N–5°S	140°W
		September 10–September 17, 1996	8°S–8°N	125°W
		October 6–October 24, 1996	8°N–8°S	110°W, 95°W
		November 28–December 15, 1996	8°N–8°S	170°W, 180°
	1997	February 7–February 26, 1997	8°N–8°S	95°W, 110°W
		April 2–April 9, 1997	8°N–2°S	125°W
		April 14–April 17, 1997	0°–8°N	140°W
		May 20–June 27, 1997	5°S–8°N	170°W, 180°
		August 4–August 21, 1997	8°N–8°S	95°W, 110°W
		October 4–October 25, 1997	8°N–8°S	125°W, 140°W
		November 10–December 4, 1997	8°N–8°S	155°W, 180°
		December 4–December 12, 1997	8°N–2°S	170°W
	1998	February 14–May 6, 1998	8°N–8°S	95°W, 110°W
		April 24–April 30, 1998	10°N–2°S	125°W
		May 9–May 14, 1998	2°S–5°N	140°W
		June 5–June 16, 1998	10°N–5°S	155°W
		June 19–June 26, 1998	8°S–5°N	170°W

Table 1 (*continued*)

Organization	Cruise name	Cruise dates	Latitude	Longitude
		July 18–July 26, 1998	8°S–10°N	180°
		September 14–September 22, 1998	8°N–8°S	125°W
		September 25–October 4, 1998	5°S–9°N	140°W
AOML/NOAA, USA	Ronald Brown TAO Cruise	October 22–November 10, 1998	8°N–8°S	95°W, 110°W
PMEL/NOAA, USA	Ka'imimoana TAO cruises	October 23–November 3, 1998	8°N–0°	155°W
		December 2–December 6, 1998	2°S–8°N	170°W
		November 21–November 29, 1998	8°N–8°S	180°
	1999	January 30–February 5, 1999	8°N–2°S	140°W
	Ka'imimoana TAO cruises	February 10–February 16, 1999	5°S–10°N	125°W
		May 7–May 15, 1999	6°N–8°S	110°W
		May 18–May 27, 1999	8°S–8°N	95°W

latitudes (e.g., Yu and Reinecker, 1998), and other synoptic scale disturbances. These wind events also excite equatorial Kelvin waves that propagate eastward across the basin in 1–2 months depressing the thermocline (as measured by the depth of the 20°C isotherm in Fig. 1) in the eastern Pacific. A deepened thermocline favors development of warm surface temperatures since the deep cold-water reservoir that feeds upwelling in the equatorial cold tongue is pushed down to greater depth. Therefore, the cold tongue weakens or fails to develop in the boreal summer and fall of an El Niño year. In the western Pacific warm pool, on the other hand, the thermocline shoals due to the excitation of equatorial Rossby waves generated by the weakened trade winds during the mature phase of the El Niño. The net result of these processes on ocean thermal structure is to flatten the thermocline along the equator, and greatly reduce the normal east-west sea-surface temperature (SST) gradient.

El Niños typically terminate in the boreal spring with the return to normal of the easterly trade winds and the resumption of equatorial upwelling. In many instances, the ocean-atmosphere system overshoots normal equilibrium conditions though, and a cold La Niña develops. A particularly striking example of the switch from El Niño to La Niña occurred in May–June 1998, when trade winds abruptly returned to near normal strength in the eastern Pacific and SSTs in the equatorial cold tongue plummeted 8°C in only 30 days (McPhaden, 1999).

2. Historical background

2.1. Western pacific warm pool

The warm-pool region of the western equatorial Pacific is generally characterized by surface temperatures that exceed 28.5°C, lower salinities, and surface waters that are depleted in nutrients. Precipitation is much larger than evaporation in the warm pool so that surface salinity decreases from east to west. The upwelling of cold waters, rich in nutrients and carbon dioxide that is characteristic of the eastern equatorial Pacific, is not observed. This is largely due to the fact that the thermocline depth increases from east to west, and that, in the west, the SE tradewinds are much less dominant and are often interrupted by episodic westerly winds resulting from the MJO (Madden and Julian, 1971, 1972). These westerly winds produce convergence and downwelling at the equator, although they can result in upwelling a few degrees north and south of the equator (Mackey et al., 1997).

Historically, this led to the assumption that the western Pacific had a deep mixed layer and was similar to the oligotrophic subtropical gyres of the major ocean basins. However, this is an

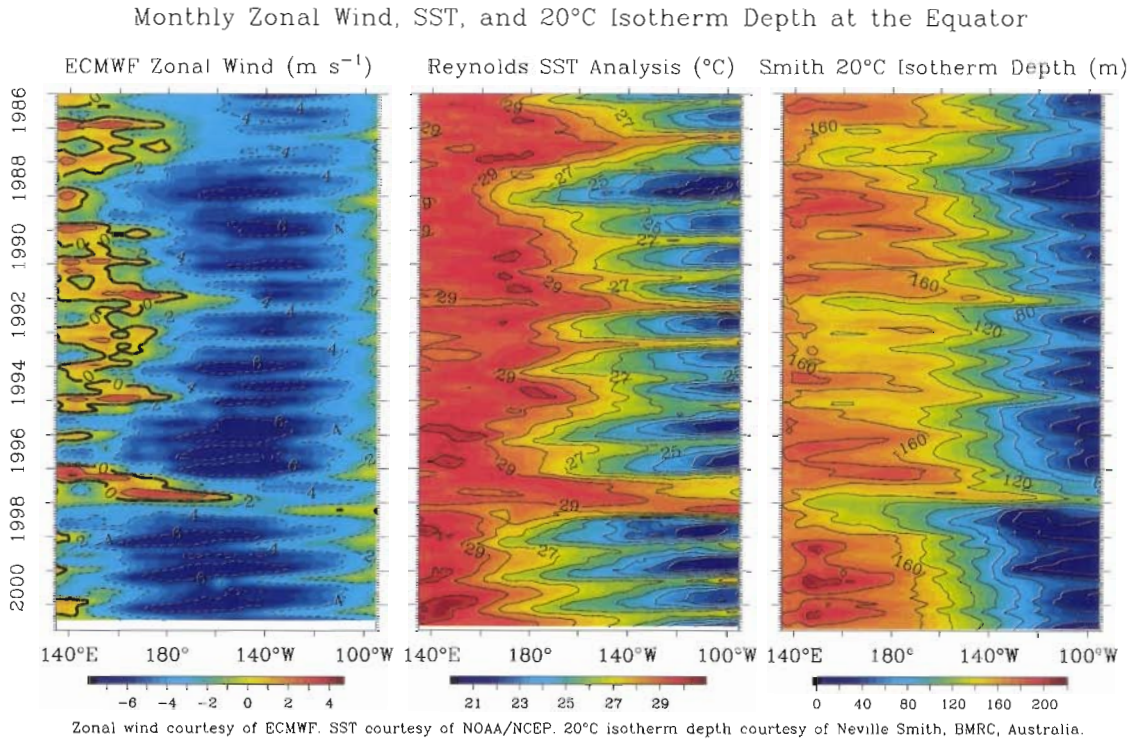

Fig. 1. Time-longitude distributions of; (a) zonal winds (in m s^{-1}); (b) SST (in°C); and (c) 20°C isotherm depth (in m) from 1986 to 2001. The analysis is based on monthly averages between 2°S and 2°N from the time-series data from the TAO/TRITON array.

oversimplification since it was shown in the 1980s that the mixed layer was often much shallower than the thermocline and was separated from it by one or more haloclines. The region between the mixed layer and the top of the thermocline has been called the 'barrier layer.' It is frequently 30–40 m thick (Lindstrom et al., 1987; Lukas and Lindstrom, 1991; Ando and McPhaden, 1997), although it can be up to 100 m thick. The barrier layer is prominent in regions of heavy precipitation and near the equator and can be formed by local fresh-water fluxes at the air–sea interface, by low-salinity surface waters flowing from west to east (Lukas and Lindstrom, 1991), or by the subduction of higher-salinity (density) water flowing to the west in the South Equatorial Current (Roemmich et al., 1994).

While surface chlorophyll concentrations (phytoplankton biomass) are low in the warm pool, the depth-integrated concentrations of chlorophyll are comparable to the eastern Pacific. However, the net productivity is much less since much of the chlorophyll is found deep in the water column, near or below the top of the thermocline, where the light level falls to 1–10% of the surface irradiance and low concentrations of nitrate ($\sim 1\,\mu mol\,l^{-1}$) are observed (Mackey et al., 1995). The barrier layer provides an effective barrier between the top of the nutricline and the mixed layer so that production in the mixed layer must be predominantly due to the use of recycled nutrients. The recycling of nutrients in the mixed layer via microbial processes also must lead to a recycling of CO_2.

Under non-El Niño conditions, upwelling of cold waters, rich in CO_2, does not occur in the western equatorial Pacific so that high values of pCO_{2sw} are not found there. The low phytoplankton biomass in the mixed layer and the recycling of nutrients in the western equatorial Pacific imply that biological processes have only a small effect on pCO_{2sw} (Inoue et al., 1995). Surface waters are

close to equilibrium with respect to atmospheric CO_2, and so the flux of CO_2 across the air–sea interface is also small (Inoue and Sugimura, 1992; Mackey et al., 1995; Inoue, 2000). Finally, small-scale temporal and spatial variations in CO_2 are dominated by thermodynamics and, in particular, the temperature dependence of the solubility of CO_2 so that, in general, pCO_{2sw} increases with SST (Fushimi, 1987; Inoue et al., 1987; Mackey et al., 1997).

The combination of shallow mixed layer, high precipitation, high insolation and variable water masses ensure that there is much small-scale variability in SST, sea-surface salinity (SSS) and pCO_{2sw}. Variations of 1.5°C in SST and 40 μatm in ΔpCO_{2sw} were found at 1°S, 155°E over a 10-day period (Mackey et al., 1997). The local wind stress controls the depth of the mixed layer through changes in turbulence generation, e.g., forming a new shallower halocline in light winds or deepening the mixed layer by erosion of the existing halocline in strong winds. The theoretical slope of pCO_{2sw} versus SST governed by solubility is about $4.2\%\,^{\circ}C^{-1}$ (Copin-Montegut, 1989; Takahashi et al., 1993), and although this relationship is frequently found in the warm pool (Inoue et al., 1995; Mackey et al., 1997), there are some occasions where smaller or larger gradients are found. The offsets in the different regression lines are due to mixing of different water masses with different salinity, dissolved inorganic carbon (DIC), and total alkalinity (TA) values, or to different water masses equilibrating with the atmosphere at different rates. While such an effect can be due to horizontal advection, it also can arise from vertical mixing. Since the thermocline lies deep in the water column and, since DIC and/or TA need not be constant in the barrier layer, wind-induced mixing or upwelling can lead to changes in pCO_{2sw} and increased SSS with little effect on SST. Inoue and coworkers used such SSS dependent pCO_{2sw}—SST relationships to estimate pCO_{2sw} from SST and to calculate CO_2 fluxes in the warm pool (Inoue et al., 2001). Under non-El Niño conditions, the warm-pool region acts as a weak source of CO_2 to the atmosphere with estimated fluxes that range from 0.07–$0.25\,mol\,m^{-2}\,yr^{-1}$ (Ishii and Inoue, 1995).

Longitudinal distributions of pCO_{2sw} in the central and western equatorial Pacific (FLUPAC Cruise, October 1994; Inoue et al., 1996; Ishii and Inoue, 1995) indicate zonal displacement of pCO_{2sw} on time scales of a few weeks. The displacement of this concentration gradient is related to El Niño. Fig. 2 shows the longitudinal distributions of pCO_{2sw} measured in January/February 1994 (mild-El Niño period), November/December 1994 (mild-El Niño period), January/February 1998 (El Niño period) and 1999 (non-El Niño period). During the 1997/98 El Niño event the warm water moved east of the dateline. The pCO_{2sw} in the western equatorial Pacific increased with the SST and SSS, and reached 380 μatm (Inoue et al., 2001). Surface waters with relatively high SSS (>34.5) and SST (>28.5°C) in the western equatorial Pacific were caused by the decrease of fresh-water inputs and/or the northward migration of surface waters from the southern hemisphere. During the 1986–87 and 1991–94 El Niños, however, ΔpCO_2 was fairly low and constant. During the strong 1982–83 El Niño event, the pCO_{2sw} also increased with a decrease in SST in the western equatorial Pacific due to enhanced vertical mixing/upwelling (Fushimi, 1987).

Under El Niño conditions, the thermocline in the warm pool shallows as warmer fresher water moves to the east, the westerly wind bursts increase in frequency and intensity, and SSS rises due to erosion of the top of the barrier layer and reduced precipitation. In contrast to the eastern equatorial Pacific, phytoplankton productivity increases (Radenac and Rodier, 1996) due to the uplifting of the thermocline and nutricline (Mackey et al., 1997). While primary production was enhanced along 165°E during the 1987 El Niño, the stronger density gradients limited the nutrient flux into the mixed layer, resulting in lower than normal surface chlorophyll concentrations (Radenac and Rodier, 1996). If the El Niño is sufficiently protracted or intense, the barrier layer disappears and the thermocline becomes eroded with a resulting decrease in SST. In contrast to the eastern equatorial Pacific, a negative Southern Oscillation Index (SOI) is then associated with a negative SST anomaly in the warm pool as

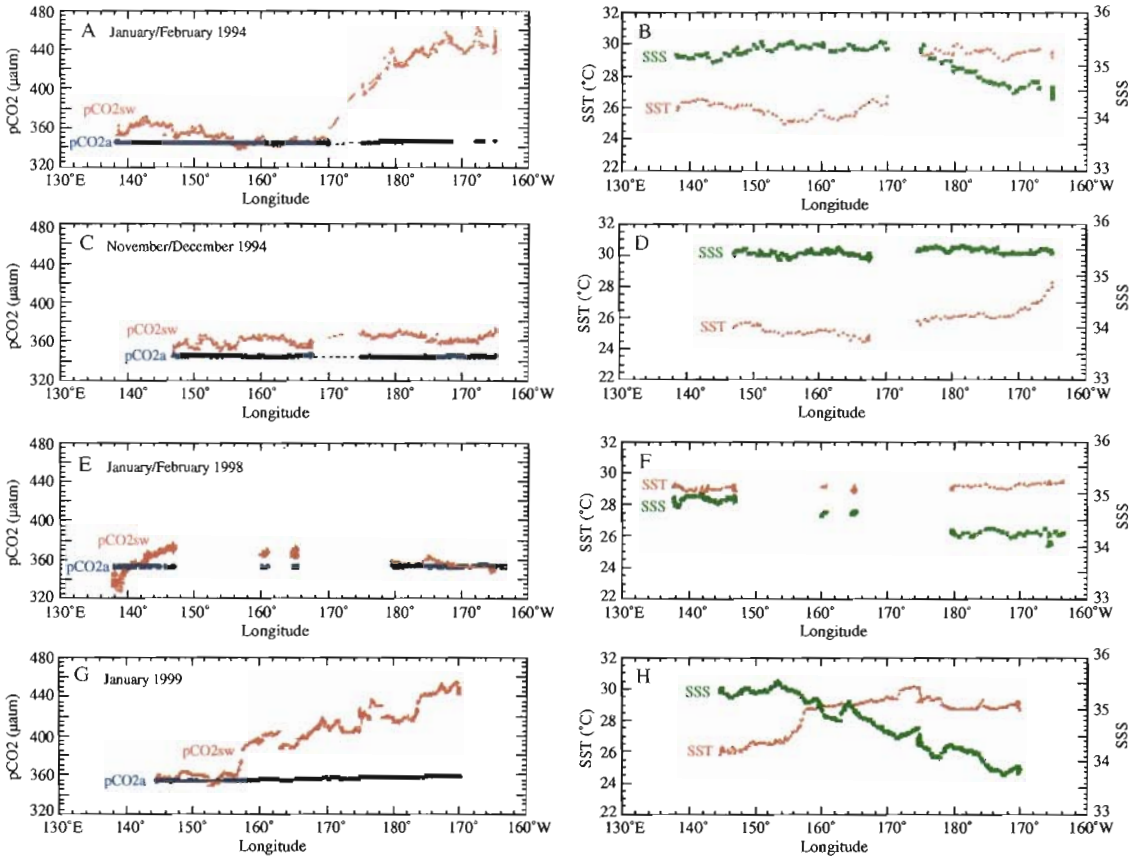

Fig. 2. Longitudinal distribution of pCO_{2sw} (left) and SST and SSS (right) along the equator in: (a) January/February 1994; (b) November/December 1994; (c) January/February 1998, and (d) January 1999. The SST data (small red solid squares) and the SSS data (large green solid squares) are modified from Inoue et al. (2001).

occurred during the 1982–83 El Niño and, intermittently, during the 1991–94 El Niño (Inoue, 2000; Rodier et al., 2000). Conversely, an increase in new production in the mixed layer during an El Niño event can lead to a lower pCO_{2sw} as was observed along 155°E in June 1992 (Mackey et al., 1997).

Under La Niña conditions, the region of equatorial upwelling extends towards the west, but it has little effect on surface salinity and temperature of the warm pool (Delcroix and Picaut, 1998). There is also little effect on the pCO_{2sw} in the warm pool, and during the 1988–89 La Niña, pCO_{2sw} at 137°E was unchanged from values observed during the 1986–87 El Niño (Inoue and Sugimura, 1992).

The longitudinal distribution of pCO_{2sw} in the central equatorial Pacific varies depending on the geographical position of the boundary between the western equatorial Pacific warm pool and the cold-tongue upwelled water (Boutin et al., 1999; Feely et al., 1999a, b). In the area of warm pool, the pCO_{2sw} is nearly constant and close to the pCO_2 in the air (pCO_{2a}). In the area of cold-tongue upwelling the pCO_{2sw} is highly supersaturated with respect to pCO_{2a}, with a maximum pCO_2 close to the equator.

The pCO_{2sw} distribution exhibits a steep change at the eastern edge of western Pacific warm water pool, where it is clearly marked by a front of SSS (Inoue et al., 1996). The pCO_{2sw} gradually decreases toward the west over spatial scales of a

few hundred kilometers (Fig. 2). Hénin et al. (1998) showed a strong variability of SSS in the western equatorial Pacific which is attributed to the zonal advection that makes the two distinct masses of water converge, resulting in a salinity front which shifts back and forth in the equatorial band. Zonal advection of the SSS front was also reported to be correlated with the Southern Oscillation Index (Picaut et al., 1996). During El Niño events, therefore, areas with low pCO_{2sw} increase because of the eastward movement of western equatorial warm pool while maintaining its salinity stratification, which results in the decrease of CO_2 outflux from the central equatorial Pacific.

During all phases and intensities of the El Niño/Southern Oscillation (ENSO) cycle, pCO_{2sw} in the warm pool is close to equilibrium with respect to the atmosphere and the region generally acts as a small source of CO_2 to the atmosphere. The major impact on the global carbon cycle is due to the changing area of the warm pool, as it shrinks during La Niña events and expands during El Niño events (Picaut et al., 1996). The border between the warm pool and the cold-tongue is delineated by the lower temperature, higher salinity, and higher pCO_{2sw} of the latter and the zonal displacement of the warm pool is strongly correlated with the SOI (Inoue et al., 1996). Inoue (2000) estimated that the CO_2 outflux per unit area was about 30-fold less in the warm pool than in the cold-tongue region in 1996. Given the small contribution of the warm pool to the global CO_2 cycle, we can now probably make reasonable estimates of the CO_2 fluxes from the warm pool directly from the SOI (Inoue et al., 1996; Rodier et al., 2000).

2.2. *Eastern equatorial pacific high nutrient low chlorophyll region*

The eastern equatorial Pacific HNLC region experiences some of the highest pCO_{2sw} values in the entire equatorial belt. The upward sloping thermocline to the east causes waters containing higher pCO_2 to be closer to the surface, which then can be entrained to the surface by local upwelling (Fig. 3). Moreover, the Peruvian upwelling system

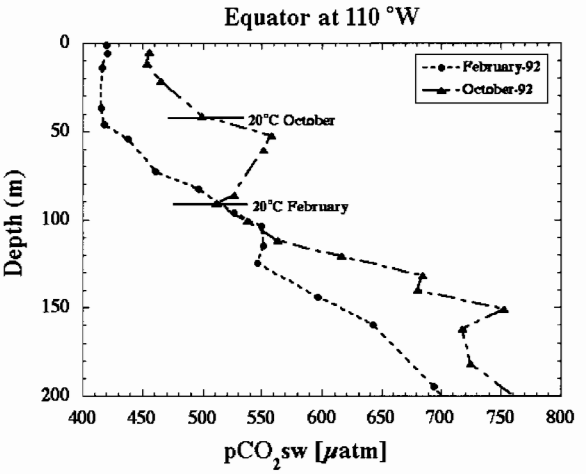

Fig. 3. pCO_{2sw} trends with depth at 110°W, 0°N for February 1992 (El Niño conditions) and October 1992 (non-El Niño conditions). The pCO_{2sw}, corrected to in situ temperature, increases rapidly with depth. The change in depth of the thermocline expressed as the depth of the 20°C isotherm (horizontal solid line) causes the pCO_{2sw} profile to deepen during El Niños, which, combined with less upwelling, decreases the pCO_{2sw} at the surface.

brings waters containing very high pCO_{2sw} (> 700–1000 μatm) to the surface. The northward-flowing Peru Current entrains this water into the SEC, east of the Galapagos, which transports the high pCO_2 water westward to about 100°W. The HNLC region shows strong asymmetry in pCO_{2sw} values across the equator. In the northern hemisphere the location of the high-gradient region from near equilibrium to highly supersaturated pCO_{2sw} values generally occurs within 1/2° or less between 5°N and the equator, depending on the position of the North Equatorial Counter Current (NECC) and/or phase of the tropical instability waves (TIW). The region between the NECC and the South Equatorial Current (SEC) is a convergence zone and an effective boundary for the spread of high pCO_{2sw} water to the north. In the Southern Hemisphere, pCO_{2sw} values remain high and fairly constant till 8–13°S, where they decrease more gradually. The instability waves on the southern edge of the equatorial Pacific and/or pulsating input from the Peru Current system apparently are the major cause of the spatial variability in the region. The westward strengthening of the NECC

and more northerly position of the convergence zone causes a more symmetrical pCO_{2sw} distribution around the equator in the central equatorial Pacific.

The boundaries of the regions with high pCO_{2sw} vary due to the phase of the ENSO cycle and to the presence of TIWs. The strong gradients of pCO_{2sw} are most prominent in the eastern Pacific where the thermocline is closest to the surface and TIW are strongest. The instability waves are a function of the shear between the eastward and westward moving currents, and thus depend on the strength of the currents. In the north the TIW are strongest in the late summer and autumn. The wavelengths are about 500–1500 km and have phase speeds of about 35–75 km d^{-1}. The TIW occasionally extend as far as 170°W and affect the temporal/spatial distributions of pCO_{2sw} in the central equatorial Pacific during non-El Niño periods.

The location of northern and southern boundaries of high pCO_{2sw} change on bi-weekly timescales because of TIW (Halpern et al., 1988). The TIW in the north have been well documented and cause significant variability in pCO_{2sw} on 100 km space scales during passage with convergence at the leading edge and divergence with higher pCO_{2sw} at the trailing edge of the feature (Lefevre and Dandonneau, 1992; Lefevre et al., 1994; Feely et al., 1994). The spatial variation in surface characteristics between the SEC and the subtropical current system to the south has received less attention, but the variability in pCO_{2sw} and to lesser extent SST is observed in several cruises (Boutin et al., 1999).

The source of high pCO_{2sw} in the SEC has not been fully resolved (Lefevre et al., 1994; Dandonneau, 1995; Wanninkhof et al., 1995; Etcheto et al., 1999). The SEC travels to the west and can be traced back to the east of the Galapagos where it might connect with the northward flowing Peru Current. Many of the analyses infer an external source of pCO_{2sw} (that is, from the upwelling system off South America) by assuming a continuous and homogeneous flow in the SEC from the Galapagos westward and assessing if the decreases in pCO_{2sw} correspond to the estimated losses by biological productivity and gas exchange. If carbon were added to the system by local upwelling, the pCO_{2sw} would increase, or decrease more slowly, to the west. Wanninkhof et al. (1995) conducted a mass balance of carbon for the region from 110°W to 140°W and concluded that during the boreal spring of 1992, during an El Niño period, the equatorial upwelling contributed little to the pCO_{2sw} levels in the SEC while during the boreal autumn the decrease to the west was much slower, suggesting local input. Large apparent oxygen utilization (AOU) at the Equator during autumn suggested active upwelling supporting this contention. Etcheto et al. (1999) emphasized the importance of the upwelling off the coast of the Americas and proposed that there is a distinct pathway for coastal upwelled water to enter into the equatorial band by showing the smooth and continuous temperature trend from Peru to the Equator. Similarly, Lefevre et al. (1994) performed an analysis in which they attributed the westward decrease in pCO_{2sw} being caused predominantly by biological activity. They suggested a stronger equatorial input towards the east rather than a separate source of the high pCO_2 water. On the other hand, Dandonneau (1995) suggested that equatorial upwelling accounts for much of the high pCO_{2sw} signal in the HNLC region. They performed an EOF analysis based on five transects of a supply ship crossing the Equator near 100°W and showed that pCO_{2sw} was strongly and positively correlated to nitrate and fluorescence and negatively with SST. This is counter to the trends caused by thermodynamics and biological uptake, and implies that the signal is dominated by local upwelling. Toggweiler et al. (1991) suggested a very limited contribution of water from upwelling off Peru to the equatorial system based on ^{14}C trends. The different conclusions as to the origin of high pCO_2 water in the SEC are attributed to the limited amount of data in the far eastern Pacific and because of changes in upwelling and circulation in response to the ENSO cycle. During normal or La Niña conditions equatorial upwelling is ubiquitous as shown by positive AOU values (Wanninkhof et al., 1995) and CFC undersaturation at the surface (Lefevre et al., 1994).

The high nutrient-low chlorophyll character of the equatorial Pacific during non-El Niño periods is generally considered to be a consequence of iron

deficiency (Behrenfeld et al., 1996; Chavez et al., 1999). As a result of this deficiency, the productive ecosystem of the equatorial Pacific is dominated by very small cells (Mackey et al., 2002), its primary productivity remains relatively low, and is controlled by grazing (Landry et al., 1997; Le Borgne et al., 2002). It takes more than 100 days for the nitrate upwelled into the mixed layer to be entirely used by photosynthesis (McCarthy et al., 1996; Stoens et al., 1999). Under such conditions, export production is only 10–20% of total primary production (McCarthy et al., 1996; Rodier and Le Borgne, 1997), and the high pCO_{2sw} values that are caused by upwelling persist for long periods because the thermodynamic effect of heat gain counteracts the combined effects of photosynthetic carbon fixation and gas exchange. Biological studies of the equatorial Pacific often stress the evenness of most oceanic properties in the South Equatorial Current: (1) primary productivity does not vary dramatically (Chavez et al., 1996); (2) the populations of photoautotrophs are dominated by picoplankton (Landry et al., 1997); (3) the physiological response of fluorescence to the diurnal cycle of irradiance follows the same pattern throughout the entire region; and (4) SeaWiFS sea-color composites exhibit less mesoscale spatial heterogeneity than other productive regions (Murtugudde et al., 1999). However, the impacts of El Niño events on physical and biological processes can cause significant drawdowns of pCO_2 in surface waters (Chavez et al., 1999).

3. Sampling and analytical methods

A comprehensive set of chemical and hydrographic data was collected on pre-JGOFS and JGOFS cruises from 1992 through 1999 by scientists from Australia, France, Japan and the United States (Table 1). During all cruises, shipboard pumping systems continuously pumped water to the oceanographic laboratory. The intakes are located near the ship's bow approximately 3–6 m below the sea surface, depending on the individual research vessel. The CO_2 mixing ratios were determined with non-dispersive analysis procedures similar to the methods described in Poisson et al. (1993), Wanninkhof and Thoning (1993) and Feely et al. (1998). The systems were run on repeat cycles during which standards, headspace samples from the equilibrator, and an ambient air samples are analyzed. Compressed gas standards flow through the infrared analyzer for calibration. The precision and accuracy is generally about 0.4% ($\sim$1–2 ppm). Although the different groups utilize minor modifications of the above procedures, the results generally agree with about 2 ppm (Körtzinger et al., 2000).

4. Results and interpretations

The high pCO_{2sw} of the equatorial upwelling system is controlled by the strength of the trade winds that in turn controls the upwelling rate (local forcing), and the depth of the thermocline regulated by large-scale undulations caused by low-frequency equatorial waves (remote forcing). The pCO_{2sw} levels increase sharply in the thermocline such that both depths from where the upwelling originates and the position of the thermocline are critical controls of surface water pCO_2 (Fig. 3).

The thermocline, often indicated by the depth of 20°C isotherm, is closest to the surface in the HNLC region and sometimes outcrops near the Galapagos Islands. Since pCO_{2sw} increases with depth in the thermocline (Fig. 3), the upwelling water to the east will contain higher pCO_{2sw} values. Near the active upwelling regions, pCO_{2sw} is dominated by the source waters and pCO_{2sw} is inversely proportional to temperature (Wanninkhof et al., 1996; Chavez et al., 1999). With time at the surface biological uptake, gas exchange and temperature will act to change the surface water pCO_2. Increases in temperature will cause pCO_{2sw} to increase, while biological production and gas transfer will decrease pCO_{2sw}. The contribution of biological productivity is one to four times greater than gas transfer for decreasing the surface water pCO_2, depending on seasons and, particularly, the phase of the ENSO (Lefevre et al., 1994; Feely et al., 1995, 1997; Wanninkhof et al., 1995; Quay, 1997; Cosca et al., 2002). Based on limited data

sets, it appears that the contribution of biology is strongest in the boreal autumn (Foley et al., 1997; Cosca et al., 2002). The pCO_{2sw} increases due to temperature increases are generally less than the decreases due to biology and gas exchange, leading to the lower pCO_{2sw} values in the boreal autumn.

4.1. The effect of ENSO on pCO_2 levels in the HNLC region

The ENSO cycle has a controlling influence on the surface pCO_2 levels by affecting the three main processes controlling large-scale pCO_2 patterns: the depth of the thermocline, the strength of the winds, and the edge of the warm pool. The eastern edge of the warm pool, which effectively caps off the upwelling system moves east of the dateline during El Niño periods. The reduced tradewinds in the eastern equatorial Pacific during the El Niños decrease the upwelling rate. Deepening of the thermocline further reduces the surface pCO_2 levels. Boutin et al. (1999) suggested that for the 0–5°S region the changing size of the warm pool is about twice as important as changes in pCO_{2sw} due to upwelling in depressing the equatorial CO_2 efflux during El Niños.

The overriding control on trends of pCO_2 levels in the HNLC region is the ENSO cycle. The large-scale distributions of ΔpCO_2 in the equatorial Pacific are shown in Fig. 4 and a composite plot of pCO_{2sw} data along 110°W from 1992 through 1998 show the trends for the months of February to June (Fig. 5). During non-El Niño periods, springtime generally shows slightly higher ΔpCO_2 levels ($\sim 30\,\mu$atm) than the boreal autumn due to lower biological productivity. The pCO_{2sw} levels during 1992 were well below the levels of 1996 because of the prolonged 1991–94 El Niño (Fig. 5). The system restored to near normal conditions in the boreal autumn of 1992 with significantly higher pCO_{2sw}. Although the boreal spring of 1993 showed a negative SOI index, it was less negative than that of the spring of 1992 and the pCO_{2sw} levels were correspondingly higher. The boreal spring of 1996 was positive with respect to the SOI index and ΔpCO_2 levels near the equator were in the range 100–140 μatm. The lowest levels for the past decade were observed in boreal autumn of 1997 and winter of 1998 during the century's largest El Niño event when maximum ΔpCO_2 values were about 30 μatm from equilibrium compared to normal supersaturated levels of over 100 μatm.

A comprehensive set of atmospheric and surface ocean pCO_2 measurements and supporting hydrographic data for the eastern equatorial Pacific were obtained from December 1995 to May 1999. The 1995–96 cruises occurred during well-developed cold-tongue conditions (Feely et al., 1999a, b) and the 1997–98 cruises occurred during the mature phase of El Niño (Chavez et al., 1999). The 1995–96 data indicates much higher seawater pCO_2 values than the corresponding values for the mature phase of the 1997–98 El Niño (Fig. 4). While values close to equilibrium were observed north and south of the equator in the western part of the study region, the region between 8°S and 6°N had a large positive ΔpCO_2 maximum close to the equator across the entire basin during 1995–96. In contrast, the late 1997—early 1998 data indicated near equilibrium ΔpCO_2 values for the same region. The distributions of ΔpCO_2 showed interannual variability in excess of 100 μatm in the eastern Pacific, the highest since the 1982–83 El Niño (Feely et al., 1987). The region abruptly changed from El Niño to La Niña conditions in mid 1998 and seawater pCO_2 values increased by more than 100 μatm in less than 4 months (Chavez et al., 1999). This recovery of the equatorial upwelling after the 1997–98 El Niño also was marked by a strong phytoplankton bloom (Murtugudde et al., 1999), which caused a drawdown of pCO_2 (Chavez et al., 1999).

To determine how well the pCO_{2sw} levels in the equatorial upwelling region correspond to indices of physical control, comparisons are made between local anomalies either expressed as mixed-layer depth or SST anomaly. High pCO_{2sw} closely corresponds to shallow mixed layer and negative SST anomalies. This suggests that in the equatorial upwelling region local control dominates the pCO_{2sw} signal. The pCO_{2sw} near the equator is representative for the levels extending to at least to 5°S (Fig. 6). For regional pCO_{2sw} extending beyond this region additional information on the spatial variability in SST, SSS, nutrients and

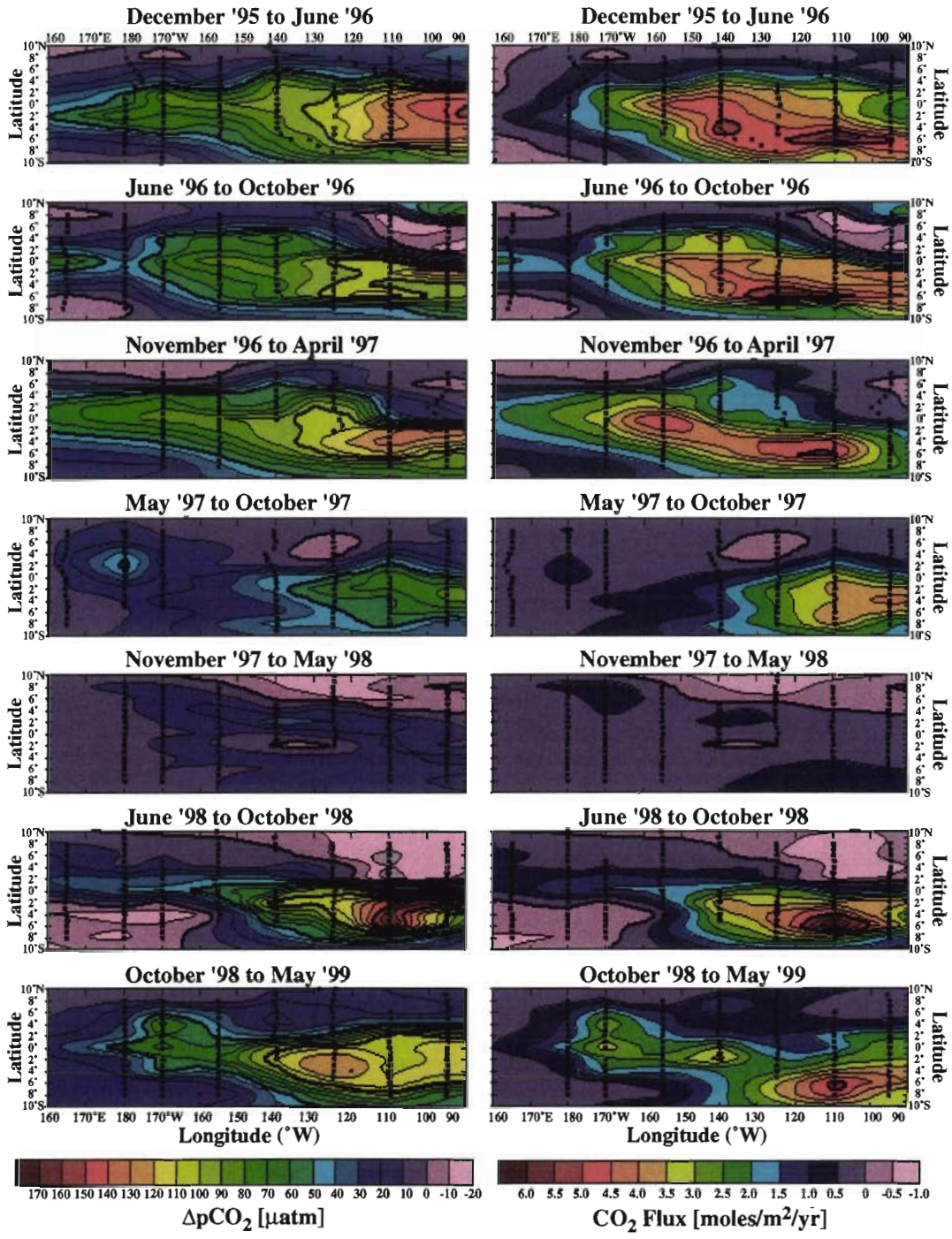

Fig. 4. The distribution of ΔpCO_2 (left) and CO_2 fluxes in $mol\,m^{-2}\,yr^{-1}$(right) in the equatorial Pacific from the December 1995 through May 1999. The lower ΔpCO_2 values during the 1997–98 El Niño event, combined with lower wind speeds, resulted in the lowest annual CO_2 flux since the 1982–83 El Niño event.

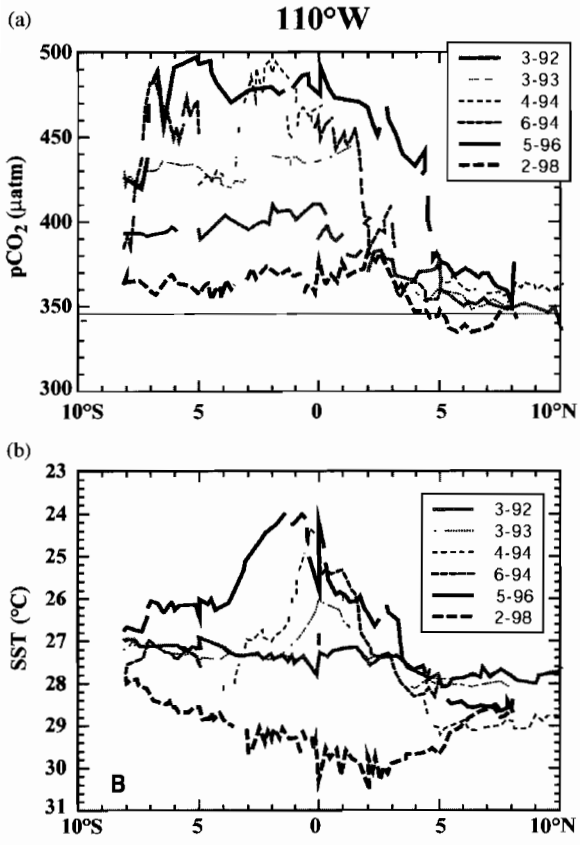

Fig. 5. Seawater pCO_2 trends (a) and SST in °C (b) along 110°W for the (boreal) spring from 1992 through 1998. (a) The thin solid line shows the approximate atmospheric pCO_2 level. The low pCO_{2sw} values correspond to El Niño periods. SST (inverted scale) shows an inverse correlation with pCO_{2sw}.

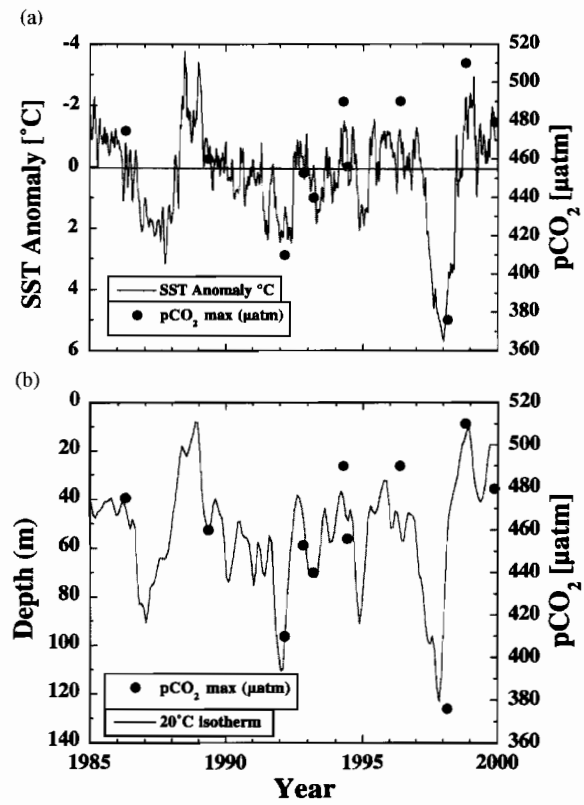

Fig. 6. Maximum pCO_{2sw} values within 1° from the Equator at 110°W and indices or proxies for the ENSO cycle plotted against time. (a) SST anomaly, and (b) 20°C isotherm depth (inverted scale).

productivity is necessary. SST, that can be obtained remotely, is a good diagnostic for changes in between 0° and 5°S (Boutin et al., 1999). SST is less of an indicator north of the equator where small SST increases can correspond to very large drops in pCO_{2sw}.

5. Discussion

5.1. Sea–air CO_2 fluxes

The properties of the water column in the eastern equatorial Pacific before and during the 1997–98 ENSO event suggest that the decrease of ΔpCO_2 was greatest during this event. The time series measurements of ΔpCO_2 recorded from the shipboard measurements (Fig. 4) show that during the mature phase of El Niño, in late 1997 and early 1998, ΔpCO_{2sw} was, on average, near or below atmospheric levels and the equatorial Pacific in region near 0, 140°W was a sink for atmospheric CO_2. This result is consistent with the mooring measurements of ΔpCO_2 CO_2 at 0, 155°W (Chavez et al., 1999). The net flux of CO_2 across the sea–air interface is the product of the gas transfer velocity, k, the solubility of CO_2, s, and the pCO_2 difference between the ocean and atmosphere (pCO_{2sw}–pCO_{2a}), according to the following equation:

$$F = ks(pCO_{2sw} - pCO_{2a}). \quad (1)$$

The gas transfer velocity k is parameterized with windspeed (Wanninkhof, 1992):

$$k = au_{10}^2 (Sc/660)^{-0.5}, \quad (2)$$

where a is a coefficient depending on the average duration of the wind speed, u_{10} = wind speed at 10 m height in $m\,s^{-1}$, s = the CO_2 solubility, and Sc = Schmidt number for CO_2.

Long-term records of remotely sensed wind speed and SST provide the ability to monitor the temporal and spatial variability of k and s. The product of these values is often expressed as a gas exchange coefficient $K(= ks)$ (Boutin and Etcheto, 1997). Fig. 7 shows the longitudinal distribution of K averaged between 0° and 5°S from 1985 to 1999 using wind speeds retrieved from the Geosat altimeter (1985–88), the SSMI microwave radiometer (1988–91) and the ERS scatterometer (1991–99) measurements. A large seasonal variation is observed in the eastern equatorial Pacific, with high K values in the boreal fall and winter. The largest values of K are observed in the central equatorial Pacific. Variations of the amplitude and of the position of K maximum are associated with ENSO events (Fig. 7). During warm El Niño periods (1986–87, 1992, 1997–98) the K maximum is shifted east of 140°W, whereas during cold La Niña periods K increases and is shifted westward (1988, 1998). The boundary between these relatively high K and the low K in the western equatorial Pacific ocean correlates very well with the edge of the warm pool, indicating that on average K is twice as low in the warm pool than it is in the central equatorial Pacific.

Using the observed pCO_2 and one-month averaged re-analysis wind speeds acquired from the European Centre for Medium Range Weather Forecasts, CO_2 fluxes calculated from the ship surveys are represented graphically in Fig. 4. A comparison of Fig. 7 with Fig. 4, left, shows that spatial variations of K and pCO_{2sw} are not correlated: pCO_{2sw} is maximum in the eastern region while K is maximum further west. Moreover, the highest pCO_{2sw} are near the equator while K is minimum at the equator and increases southward. This is the reason why two separate CO_2 flux maxima are often observed in the HNLC region, one near 140°W and one near 110°W with a slight depression in between (Fig. 4). The flux data show the large interannual effects of El-Niño on CO_2 exchange in the equatorial Pacific. From the near normal conditions of 1996 to the mature El Niño period during 1997–98, the average CO_2 fluxes from 10°S to 10°N and 80°W to 135°E decreased from approximately 2.0–0.3 mol C $m^{-2}\,yr^{-1}$. The high CO_2 fluxes in 1996 were due to increased surface water pCO_2 values and higher winds. We estimate that for the 1-year period of 1996 approximately 0.9 ± 0.6 Pg C as CO_2 was released to the atmosphere. In sharp contrast, for the 1-year period from the spring of 1997 to the spring of 1998, the CO_2 flux to the atmosphere was approximately 0.2 ± 0.14 Pg C over the same region. Somewhat smaller flux anomalies were observed during the 1982–83, 86–87 and 92–93 El Niño events (Table 2). These differences accounted for approximately one-third of the atmospheric anomaly during the 1992–93 El Niño. However, during the sharp decline of the equatorial Pacific CO_2 release at the beginning of the 1997–98 El Niño, the atmospheric CO_2 growth rate accelerated after an earlier decline. This change in the atmospheric growth rate of CO_2 can be explained if we assume that the decline in the CO_2 outgassing in the equatorial begins as early as 10–14 months prior to the minimum in the SOI index (Fig. 9) and that the initial decline and later stage increase in the atmospheric growth rate also are due to responses of the terrestrial biosphere. This two-process scenario is consistent with the atmospheric CO_2 inversion model results (Rayner et al., 1999).

The CO_2 outflux from the central and western equatorial Pacific (5.5°S–5.5°N, 139.5°E–159.5°W) was estimated to be 0.055 Pg C yr^{-1} in January/February 1987, 0.34 Pg C yr^{-1} in January/February 1989, 0.11 Pg C yr^{-1} in September/November 1990, and 0.027–0.038 Pg C yr^{-1} in December 1997 to February 1998, and 0.225 Pg C yr^{-1} in January/February 1999 (Inoue et al., 2001). During non-El Niño periods, the CO_2 outflux from the equatorial Pacific west of 160°W (central and western equatorial Pacific) contributes up to 30% of the total. During the decade of the 1990s, which was dominated by strong and prolonged El Niño events, the CO_2 outflux from the equatorial Pacific

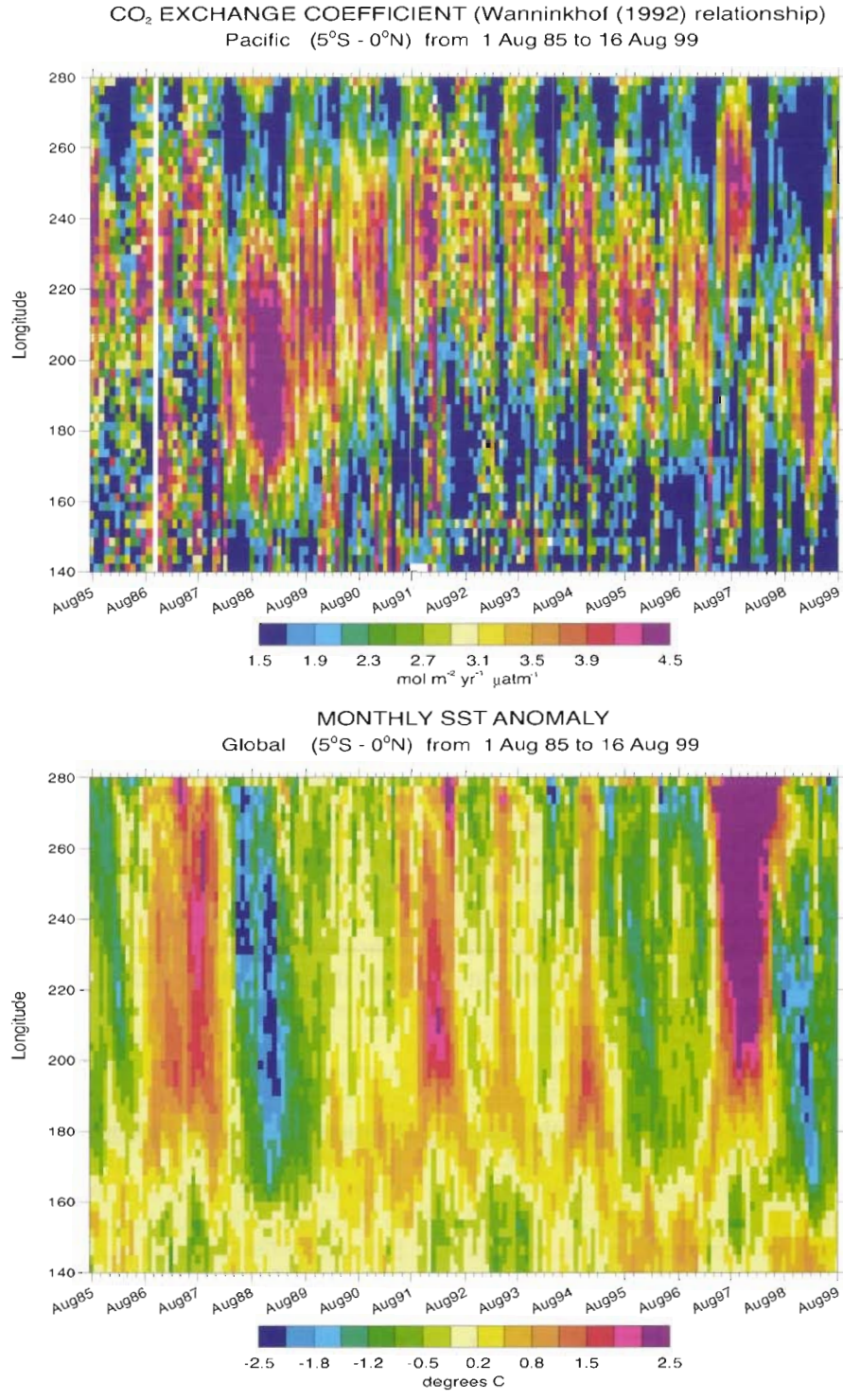

Fig. 7. Time series of K (top) and of the SST anomalies (bottom) with respect to a monthly climatology derived from the NMC analysis.

Table 2
Comparison of estimates of CO_2 sea-to-air flux from the equatorial Pacific

Region of interest	Year of study	Area $\times 10^6$ km^2	Mean ΔpCO_2 µatm	Annual flux Pg C	Reference
Non-El Niño conditions					
5°S, 5°N, 100°W, 170°E	1979–80	11	70	0.6	Keeling and Revelle (1985)
10°S, 10°N, 80°W, 150°E	1979–80	31	51	0 8	Smethie et al. (1985)
10°S, 10°N, 80°W, 130°E	1979–80	34.4	51	0.8	Takahashi et al. (1986)
10°S, 10°N, 80°W, 135°E	1984	35	60	0.6	Feely et al. (1987)
10°S, 10°N, 80°W, 120°E	1984	39	60	0.8	Volk (1989)
10°S, 10°N, 170°W, 180°	1989	35*	50	0.4	Wong et al. (1993)
5.5°S, 5.5°N, 80.5°W, 134.5°E	1989	21	79	0.96	Inoue and Sugimura (1992)
10°S, 10°N, 80°W, 135°E	1996	35	63	0.9±0.6	Feely et al. (1999a, b)
El Niño conditions					
10°S, 10°N, 80°W, 135°E	1983	35	2	0.02	Feely et al. (1987)
10°S, 10°N, 170°W, 180°	1987	35*	5	0 09	Wong et al. (1993)
5.5°S, 5.5°N, 80.5°W, 134.5°E	1987	21	31	0.4	Inoue and Sugimura (1992)
10°S, 10°N, 80°W, 135°E	1992	35	27	0.3±0.2	Feely et al. (1995)
10°S, 10°N, 80°W, 135°E	1993	35	51	0.6±0.4	Feely et al. (1999a, b)
10°S, 10°N, 80°W, 135°E	1994	35	60	0.7±0.4	Feely et al. (1999a, b)
10°S, 10°N, 80°W, 135°E	1997	35	31	0.4±0.2	Feely et al., this study
10°S, 10°N, 80°W, 135°E	1998	35	30	0.4±0.2	Feely et al., this study

*Extrapolated to 35×10^6 km^2

decreased considerably as compared with that of 1980s, which may be due to anthropogenically forced changes in climate projecting primarily onto the principal patterns of natural variability (Corti et al., 1999).

The large number of in situ pCO_{2sw} measurements in the equatorial Pacific can be correlated with SST variations (Wanninkhof et al., 1996; Boutin et al., 1999; Etcheto et al., 1999; Cosca et al., 2002), and so the large-scale pCO_{2sw} and air–sea CO_2 flux variations can be determined from long-term satellite SST and wind-speed measurements. Fig. 8 shows the pCO_{2sw} at 100°W extrapolated as described by Etcheto et al. (1999) from weekly SST anomalies with respect to a monthly climatology of SST derived from the National Meteorological Center (NMC) analysis. The SST at 100°W lags the SST observed in the Peru upwelling by about 5 weeks. The SST-derived pCO_{2sw} at 100°W is high during the 1995–96 La Niña and close to the equilibrium with the atmosphere during the 97–98 El Niño, in agreement with underway pCO_{2sw} measurements made during this period (Fig. 4). Fig. 9 shows the time series of the CO_2 flux integrated over the equatorial upwelling region between the equator and 5°S derived using pCO_{2sw}-SST and pCO_{2sw}-SST anomaly relationships east of the warm pool (Boutin et al., 1999; Etcheto et al., 1999). Since both K and pCO_{2sw} are lower in the western equatorial Pacific than in the upwelling region, this flux is expected to be very close to the flux integrated over the whole equatorial Pacific ocean between 0° and 5°S. Boutin et al. (1999) make use of relationships between SST, SST anomalies with pCO_{2sw}, independent of time while Cosca et al. (2002) derive seasonal SST-pCO_{2sw} relationships. The flux obtained east of the warm pool using these two methods is very similar; the flux average over the 15 years is nearly the same, approximately 0.18 Pg C yr^{-1}, and the absolute difference is always less than 0.03 Pg C yr^{-1}.

The pCO_{2sw} distributions we obtain from these satellite extrapolations are also useful for validating independent model estimates. As an example, Fig. 10 compares the 1982–99 time series of the ΔpCO_2 anomaly averaged over the entire equatorial band derived with the extrapolation scheme of

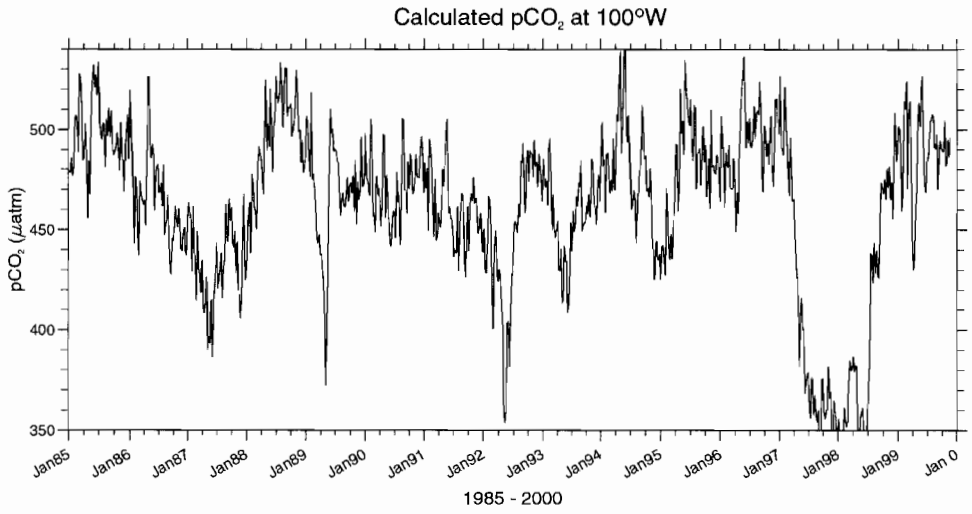

Fig. 8. Time series of pCO_{2sw} extrapolated at 100°W.

Boutin et al. (1999) and Etcheto et al. (1999) with the model of Le Quéré et al. (2000) updated with the biology model of Aumont et al. (1999) and initialized with observations (Levitus et al., 1993; Goyet et al., 2000). Both estimates reproduce interannual anomalies, such as the large decreases of ΔpCO_2 during El Niño events. Nevertheless, some disagreements still remain. During the recent 1997–98 El Niño the drawdown simulated by the model is only about two-thirds of the one deduced from the extrapolation. The reason for this is because, towards the end of the simulation, the model underpredicts the mean ΔpCO_{2sw} and its drawdown in the eastern Pacific, while the extrapolations predict ΔpCO_{2sw} that are in agreement with the in-situ measurements throughout the period of interest (Figs. 4 and 10). The mean ΔpCO_2 value is 17 µatm lower in the model than in the extrapolation because of a drift of the model as a function of time. This comparison demonstrates the complementary nature of both approaches: the extrapolations allow us to estimate precise ΔpCO_2 at time and space scales comparable with the model scales but only over specific regions well covered with in-situ measurements. On the other hand, models allow us to make estimates over larger areas but need to be validated in selected regions using extrapolated data.

In the future, multiple satellite missions should provide good quality measurements of wind speed and SST, to allow continued monitoring of CO_2 fluxes. Moreover, the monitoring of ocean color has started with SeaWiFS. Combining the ocean color data with concurrent in situ pCO_2 measurements should provide us with more precise pCO_{2sw} parameterizations, since ocean color is complementary to the SST information as it acts both as a tracer of the biological activity as well as a tracer of the ocean circulation.

5.2. *Long-term trend of pCO_2 in the equatorial Pacific*

A few studies of long-term trends of pCO_{2sw} in the equatorial Pacific suggest that it is increasing in response to the atmospheric CO_2 increase. Long-term trends of pCO_{2sw} that have shown an increase parallel with pCO_{2a} have been reported in the HNLC region. For example, Feely et al. (1999a, b) estimated the long-term trend of pCO_{2sw} using a pCO_{2sw}-SST relationship and concluded that the entrained subtropical water, which is injected into the upwelled water, has been recently exposed to, and equilibrated with, the atmosphere. For the region north of the equator the long-term trend of pCO_{2sw} in the western North Pacific has been measured every boreal winter from 1981 through

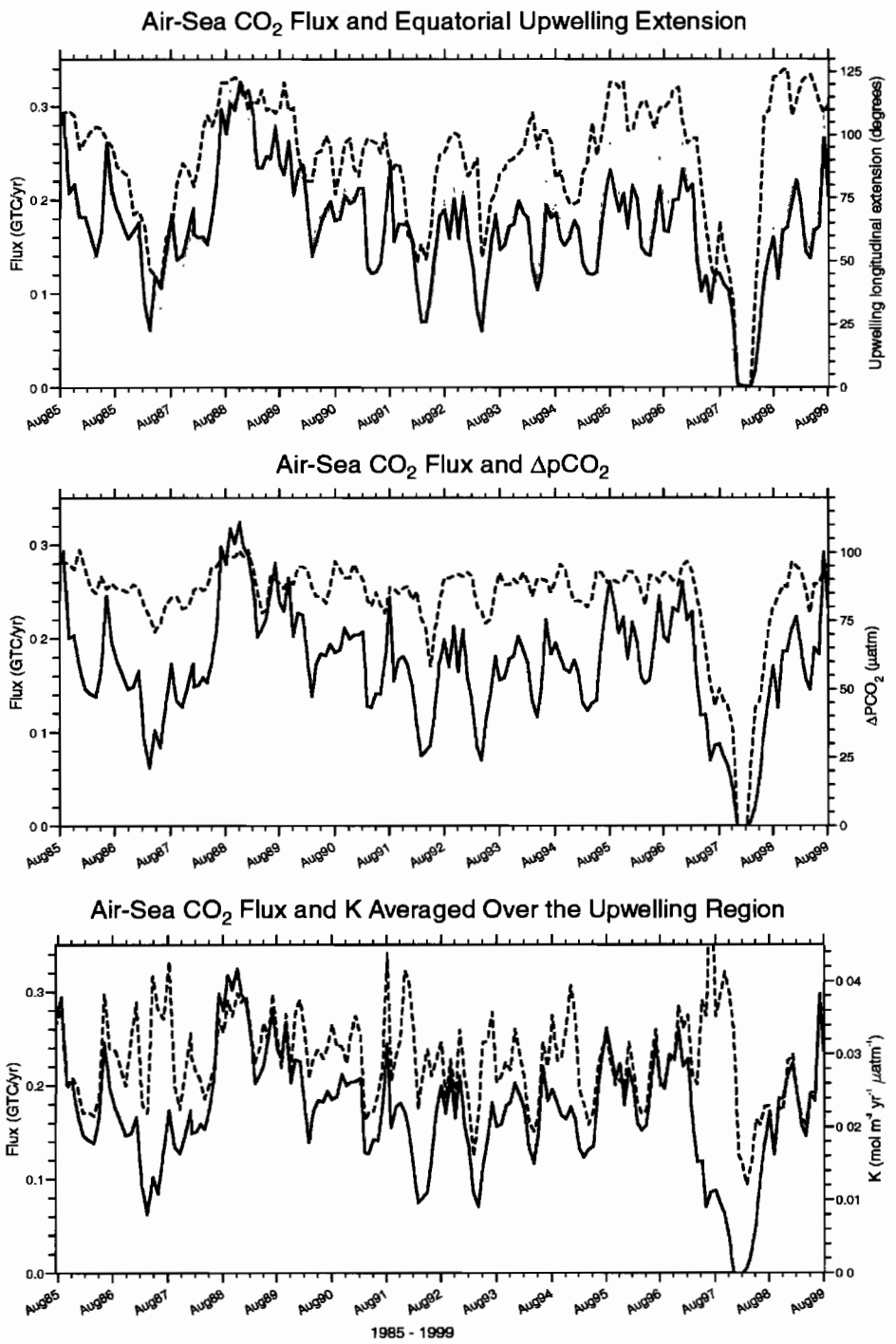

Fig. 9. Time series of the flux integrated over the upwelling region between 0° and 5°S, derived with the (Boutin et al., 1999) relationship (thick continuous line) and with the (Cosca et al., 2000) relationship (top, thin continuous line). The dashed lines indicate the upwelling longitudinal extension (top), ΔpCO_2 average (middle) and K average(bottom).

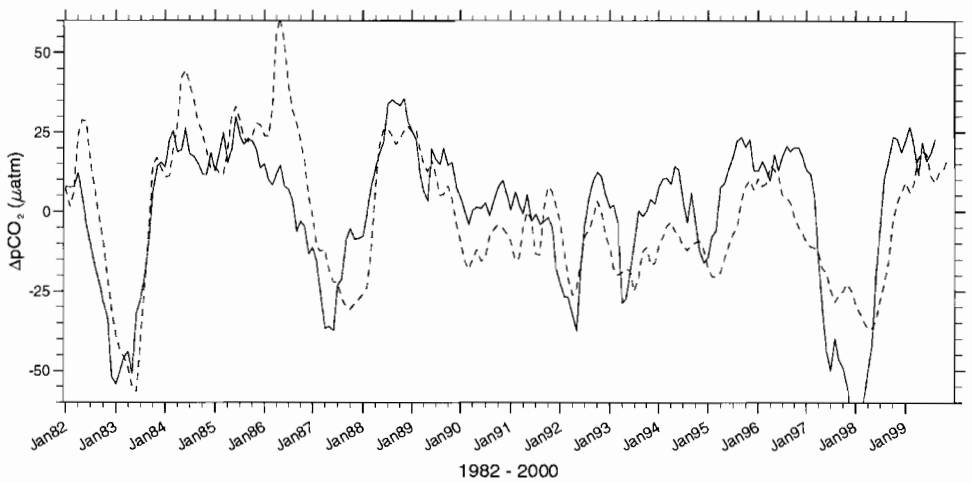

Fig. 10. Mean ΔpCO_2 anomaly averaged between 140°E and 80°W and between 0° and 5°S derived by a biogeochemical ocean model (Le Quéré et al., 2000, with modifications as described in the text) (dashed line) and by SST based relationships applied to satellite data (Boutin et al., 1999; Etcheto et al., 1999) (continuous line).

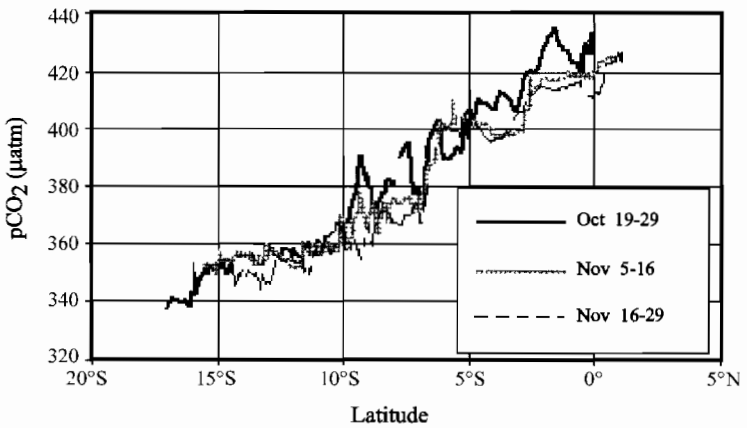

Fig. 11. Sea-surface pCO_{2sw} meridional distribution observed in the Central Pacific (150°W) during three transects in October–November 1994 (Le Borgne et al., 1995; Metzl and Brès, 1996)

1997 (JMA, 1999). By assuming a linear trend, the rate of pCO_{2sw} increase in the western North Pacific has been estimated to be $1.6 \pm 0.4\,\mu atm\,yr^{-1}$. Similar results were obtained at stations BATS and HOT situated in subtropical waters of the Northern Hemisphere (Bates et al., 1996; Winn et al., 1998).

The distribution of pCO_{2sw} determined along 150°W between Tahiti and Hawaii has been well documented (Weiss et al., 1982; Keeling, 1993; Goyet and Peltzer, 1994). Fig. 11 shows the continuous pCO_2 measurements during the three transects occupied at 150°W in October/November 1994 during the FLUPAC and OLIPAC expeditions. From week to week, very similar distributions were recorded: a relatively homogeneous pCO_{2sw} in the band 16°S–10°S, a zone of higher variability between 10°S and 4°S, and a pCO_{2sw} maximum reached near the equator (2°S in October, 1°N in November). For the long-term comparison of sea surface pCO_2 distribution, the late November 1994 FLUPAC and OLIPAC data are compared with those obtained in November 1979 (Weiss et al., 1994) corresponding to the same

season and climatic conditions. Fifteen years separates the two data sets. The atmospheric concentrations measured during these cruises were 337.1 (±0.4) ppm in 1979 and 359.5 (±0.2) ppm in 1994.

In order to elucidate the long-term trend of pCO_{2sw} caused by the anthropogenic pCO_2, the effects of thermodynamics, biological activity and ocean dynamics should be removed from observed changes in pCO_{2sw} measured at different times and locations. Air–sea pCO_2 exchange, thermodynamics (SST and SSS), ocean dynamics, and biological activities are factors controlling spatial/temporal variations in pCO_{2sw} (Poisson et al., 1993). Although there are some local differences, such as that at 5°S, which is near a frontal zone, the large-scale meridional distributions in November 1979 and November 1994 are very similar. The large differences observed near the equator could be related to change in vertical velocity (upwelling of enriched sub-surface CO_2) associated with El Niño events. November 1994 was situated in a relatively modest El Niño phase. Observed SST show positive anomalies at 150°W, whereas in November 1979 no large SST anomalies were observed along 150°W. The SST difference between the two cruises was about 1°C warmer at the equator in 1994. In the eastern and central equatorial Pacific both spatial and temporal variations in pCO_{2sw} are negatively correlated with SST, while in the subtropics pCO_{2sw} is positively correlated with SST mainly due to the effect of thermodynamics. It has been demonstrated, for many oceanic regions, that either directly or indirectly factors controlling pCO_{2sw} are correlated with seawater temperature (Watson et al., 1991; Metzl et al., 1995; Goyet et al., 1998; Lee et al., 1998). Therefore, comparing pCO_{2sw} data at the same SST within the same water mass could allow us to estimate the long-term trend. This is based on the assumption that processes controlling pCO_{2sw} are the same function of temperature over time, provided there are no changes in alkalinity. Fig. 12 shows the apparent temperature dependence of pCO_{2sw} in the SEC measured in November 1979, October 1990 (Ishii and Inoue, 1995), and November 1994. If we compare pCO_{2sw} within the SST range between

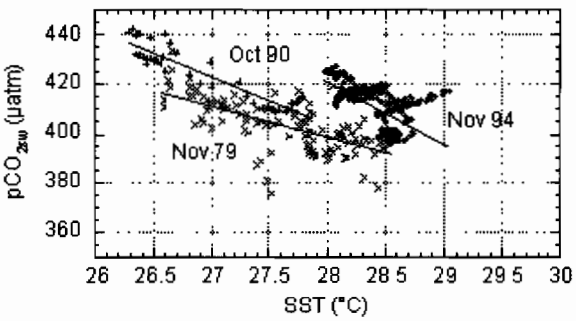

Fig. 12 Temperature dependence of pCO_{2sw} in the SEC (150°W–159°W, 1°N–5°S). ×: November1979, +: October 1990, and solid circle: November 1994. Solid lines show the linear relationship between pCO_{2sw} and SST: $pCO_{2sw} = -12.85 \times SST + 757.9$ ($r = 0.686$) for November 1979, $pCO_{2sw} = -18.97 \times SST + 935.0$ ($r = 0.919$) for October 1990, $pCO_{2sw} = -25.06 \times SST + 1122\,3$ ($r = 0.620$).

26.5 and 28.0°C observed for the period between November 1979 and October 1990, pCO_{2sw} measured in October 1990 was high compared with that of November 1979. The linear pCO_{2sw}-SST relationship gives the pCO_{2sw} increase of about 9–15 µatm for the SST range from 26.5°C to 27.5°C. Fig. 12 also shows that pCO_{2sw} along 150°W in November 1994 was approximately 16–22 µatm higher than those of November 1979 for the SST range from 28°C to 28.5°C. November 1994 was within the El Niño period, and as a whole pCO_{2sw} is negatively correlated with SST. It is clear that differences between pCO_2^{90} and pCO_2^{79} and between pCO_2^{94} and pCO_2^{79} could be at least partially caused by anthropogenic CO_2 invasion. However, short-term small-scale variations in pCO_{2sw} data have not been characterized well enough to elucidate the long-term trend of pCO_{2sw} in a quantitative sense.

In the subtropical zone (16°S–12°S), the temperature-normalized pCO_{2sw} ($pCO_2^{79/94}$) distributions are homogeneous, as in 1994 (Fig. 13). In this region the average difference (pCO_2^{94}–$pCO_2^{79/94}$) is approximately 16 µatm. The rate of increase in the ocean, approximately 1 ± 0.3 µatm yr^{-1}, is similar to that found by Feely et al. (1999a, b) for the equatorial region for data collected in the boreal spring for the period from 1961 through 1996. The oceanic pCO_2 increase rate is about the same as that found in the Southern Indian gyre (Metzl

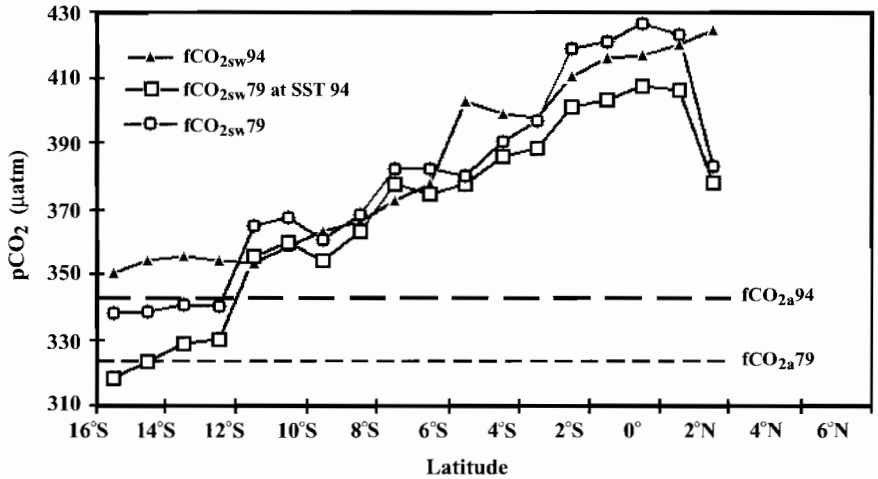

Fig. 13. Oceanic and atmospheric pCO_{2sw} observed in November 1979 (small open squares, NORPAX cruise, Weiss et al , 1994) and November 1994 (filled triangles, OLIPAC cruise) along 150°W in the Central Pacific. The continuous measurements have been averaged for each degree in latitude. Large open squares show the normalized pCO_{2sw} measured in 1979 projected to SST measured in 1994. In the subtropical region, the pCO_{2sw} increases 16 µatm over 15 years.

et al., 1998) but is somewhat lower than computed for the western North Pacific for the period 1981–97 and western South Pacific (Inoue et al., 1995, 1999). These results, based on observations, seem to suggest that invasion of anthropogenic pCO_2 might be different at basin-wide scales.

In the tropical and equatorial region, the ENSO cycle causes a strong interannual signature such that detection of the anthropogenic CO_2 signal will be difficult. By comparing our results with large-scale ocean models, we may be able to understand more clearly what the observations suggest for the long-term trends in oceanic pCO_2 variations. An example of such data/model comparison is shown in Fig. 14 in which the differences pCO_2^{94}–pCO_2^{79} along 150°W are plotted for both observations and model outputs (Le Quéré et al., 2000). The model is a version of the global carbon cycle model from IPSL, and is forced interannually for the years 1979–98. The comparison presented in Fig. 14 shows that the large-scale model captures a relatively coherent distribution of the long-term pCO_2 changes, with differences between 1979 and 1994 approaching 20–30 µatm in the subtropical and equatorial waters, and much lower differences around 10°S–5°S, as in the observations. As mentioned previously, the band 10°S–5°S lies within a pCO_2 gradient for which the mesoscale variability is not reproduced by the large-scale model. However, we learn that both the observations and models show a coherent distribution of the pCO_2 differences, with a marked minimum at 5°S. The dynamical field produced by the model suggests that this minimum is likely related to a decadal change in the zonal advection of the SEC. The model indicates that the SEC was stronger in November 1979 compared to November 1994, transporting westward more dissolved inorganic carbon (DIC) in the central Pacific. This natural variability in the advective field certainly masked the detection of anthropogenic pCO_2 in ocean surface waters in this latitude band. Although this comparison is only for the period of observations, estimates of anthropogenic pCO_2 should account for natural variations of the oceanic carbon cycle as well as the anthropogenic signals.

6. Conclusions

The data presented here show that the sea–air flux of CO_2 from the equatorial Pacific diminished by 0.4–0.7 Pg C yr^{-1} during every El Niño event

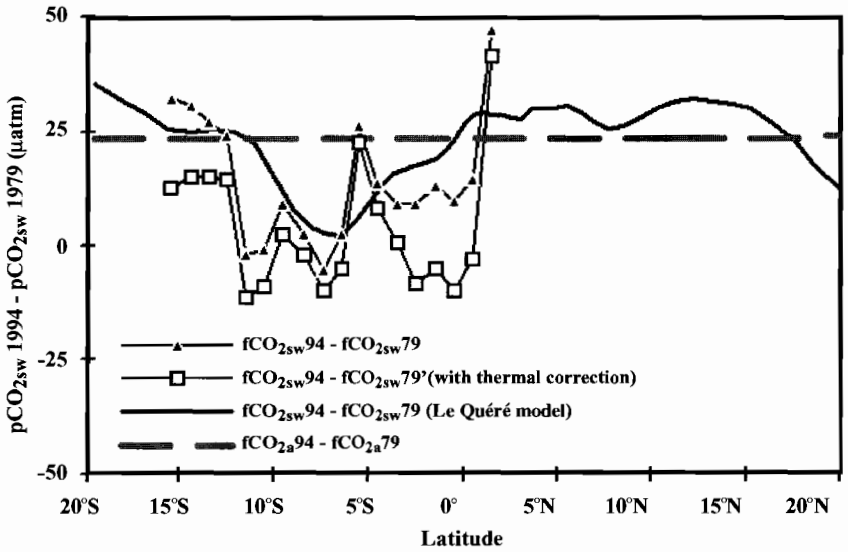

Fig. 14. Meridional distribution of the differences of oceanic pCO_{2sw} measured in 1979 and 1994 (triangles), the differences of the normalized pCO_{2sw} (open squares), and the pCO_{2sw} differences (1994–1979) obtained in an interannual simulation based on a large-scale ocean carbon model Oceanic (Le Quéré et al., 2000). The atmospheric pCO_2 difference is also shown (gray broken line).

since 1979. The direction of this change is always to reduce the usual flux of 0.8–1.0 Pg C yr^{-1} outgassed by the ocean. This variability is primarily controlled by the physical processes associated with the ENSO cycle: the reduction of the equatorial upwelling, the decrease in wind speed over the CO_2-rich water, and the migration of the warm pool from the western to the central equatorial Pacific during the warm phase of the ENSO cycle. On a basin scale, warming and the reduction in biological productivity during the ENSO warm phase oppose the physical processes—but never dominate them in controlling the sea–air CO_2 flux. The interannual variability of CO_2 fluxes in the equatorial Pacific plays a significant role in affecting the annual rate of growth of CO_2 in the atmosphere, which usually shows an early decrease followed by an increase of 2–6 Pg C yr^{-1} later in the El Niño event. Thus the magnitude of the changes in CO_2 generated by the equatorial Pacific can be up to about 30% of the observed atmospheric variability. Since the decade of the 1990s was dominated by multiple El Niño events, the outgassing of CO_2 was significantly reduced as compared with previous decades. The implication of these findings is that the equatorial Pacific upwelling zone is an important region for studying climate feedbacks over decadal time scales.

Acknowledgements

This research was supported by the NOAA Climate and Global Change Program as part of the Global Carbon Cycle program (Contract Number GC-99-220). We thank Dr. Lisa Dilling of the NOAA Office of Global Programs and Dr. Donald Rice of the US National Science Foundation for their efforts in the coordination of this JGOFS project. We also thank Robert Le Borgne and two anonymous reviewers for very helpful comments on this paper. We wish to acknowledge support from the European Communities contract ENV4-CT95-0132 (ESCOBA), the France JGOFS and INSU/PROOF programs, and the Japan JSOBGGA/GCMPAS programs. Contribution Number 2210 from the Pacific Marine Environmental Laboratory and Number 769 from the University of Washington Joint Institute for the Study of the Atmosphere and Oceans. This is U.S. JGOFS contribution number 798.

References

Ando, K., McPhaden, M.J., 1997. Variability of surface layer hydrography in the tropical Pacific Ocean. Journal of Geophysical Research 102, 23063–23078.

Archer, D.E., Takahashi, T., Sutherland, S., Goddard, J., Chipman, D., Rodgers, K., Ogura, H., 1996. Daily, seasonal, and interannual variability of sea-surface carbon and nutrient concentration in the equatorial Pacific Ocean. Deep Sea Research II 43, 779–808

Aumont, O., Orr, J.C., Monfray, P., Madec, G., Maier-Reimer, E., 1999. Nutrient trapping in the equatorial Pacific: the ocean circulation solution. Global Biogeochemical Cycles 13 (2), 351–369

Bates, N.R., Michaels, A.F, Knap, A.H., 1996. Seasonal and interannual variability of the oceanic carbon dioxide species at the US JGOFS Bermuda Atlantic Times-series Study (BATS) site Deep Sea Research II 43 (2–3), 347–383.

Behrenfeld, M.J., Bale, A.J., Kolber, Z.S., Aiken, J., Falkowski, P G., 1996. Confirmation of iron limitation of phytoplankton photosynthesis in the equatorial Pacific Ocean. Nature 383, 508–511.

Boutin, J., Etcheto, J., 1997 Long term variability of the air–sea CO_2 exchange coefficient: consequences for the CO_2 fluxes in the equatorial Pacific Ocean. Global Biogeochemical Cycles 11, 453–470.

Boutin, J., Etcheto, J., Dandonneau, Y., Bakker, D C.E., Feely, R.A., Inoue, H Y., Ishii Ling, R.D., Nightingale, P.D., Metzl, N., Wanninkhof, R., 1999. Satellite sea surface temperature: a powerful tool for interpreting in situ pCO_2 measurements in the equatorial Pacific Ocean Tellus 51B, 490–508.

Chavez, F.P., Buck, K.R., Service, S.K., Newton, J., Barber, R T, 1996 Phytoplankton variability in the eastern and central tropical Pacific. Deep Sea Research II 43, 835–870.

Chavez, F.P., Strutton, P.G, Friederich, G.E., Feely, R.A, Wanninkhof, R., Feldman, G., Foley, D., McPhaden, M J., 1999. Biological and chemical response of the equatorial Pacific Ocean to climatic forcing during the 1997–1998 El Niño. Science 286 (5447), 2126–2131.

Copin-Montegut, C., 1989. A new formula for the effect of temperature on the partial pressure of CO_2 in seawater—erratum. Marine Chemistry 27, 143–144.

Corti, S., Molteni, F., Palmer, T.N., 1999. Signature of recent climate change in frequencies of natural atmospheric circulation regimes. Nature 398, 799–802

Cosca, C.E, Feely, R.A, Wanninkhof, R., Boutin, J., Etcheto, J., McPhaden, M.J., Chavez, F P, Strutton, P.G, 2002. Seasonal and interannual variations of the fCO_2-SST relationships for the central and eastern Equatorial Pacific. Marine Chemistry, submitted

Dandonneau, Y., 1995. Sea-surface partial pressure of carbon dioxide in the eastern equatorial Pacific (August 1991 to October 1992). a multivariate analysis of physical and biological factors. Deep Sea Research II 42, 349–364.

Delcroix, T., Picaut, J., 1998. Zonal displacement of the western equatorial Pacific "fresh pool". Journal of Geophysical Research C 103, 1087–1098

Etcheto, J, Boutin, J., Dandonneau, Y., Bakker, D.C.E., Feely, R.A, Ling, R.D., Nightingale, P.D, Wanninkhof, R, 1999. Air–sea CO_2 flux variability in the equatorial Pacific Ocean near 100°W. Tellus 51B, 734–747.

Feely, R A., Gammon, R.H, Taft, B.A., Pullen, P.E., Waterman, L.S., Conway, T.J., Gendron, J.F., Wisegarver, D.P., 1987. Distribution of chemical tracers in the eastern equatorial Pacific during and after the 1982–83 El Niño/Southern Oscillation Event. Journal of Geophysical Research 92 (C6), 6545–6558

Feely, R.A., Wanninkhof, R., Cosca, C E., McPhaden, M J., Byrne, R H., Millero, F.J., Chavez, F.P., Clayton, T, Campbell, D.M., Murphy, P.P., 1994. The effect of tropical instability waves on CO_2 species distributions along the equator in the eastern equatorial Pacific during the 1992 ENSO event. Geophysical Research Letters 21 (4), 277–280.

Feely, R.A., Wanninkhof, R., Cosca, C.E, Murphy, P.P., Lamb, M.F, Steckley, M.D., 1995. CO_2 distributions in the equatorial Pacific during the 1991–92 ENSO Event. Deep Sea Research II 42, 365–386.

Feely, R A., Wanninkhof, R., Goyet, C., Archer, D.E., Takahashi, T, 1997. Variability of CO_2 distributions and air–sea fluxes in the central and eastern equatorial Pacific during the 1991–1994 El Niño. Deep Sea Research II 44 (9–10), 1851–1867.

Feely, R.A., Wanninkhof, R, Milburn, H.B, Cosca, C E., Stapp, M., Murphy, P.P, 1998 A new automated underway system for making high precision pCO_2 measurements aboard research ships. Analytica Chimica Acta 377, 185–191

Feely, R.A., Wanninkhof, R., Takahashi, T, Tans, P P, 1999a. Influence of El Niño on the equatorial Pacific contribution to atmospheric CO_2 accumulation. Nature 398, 597–601.

Feely, R.A., Wanninkhof, R., McPhaden, M.J, Meinen, C.S., Boutin, J., Etcheto, J, 1999b The role of ENSO on the phasing of the CO_2 signal in the Equatorial Pacific EOS Transactions, American Geophysical Union Supplement 80 (49), 279.

Foley, D.G., Dickey, T.D., McPhaden, M.J., Bidigare, R.R., Lewis, M.R., Barber, R.T., Lindley, S.T., Garside, C, Manov, D.V, McNeil, J D., 1997. Longwaves and primary productivity variations in the equatorial Pacific at 0°, 140°W Deep-Sea Research II 44 (9–10), 1801–1826.

Fushimi, K., 1987. Variation of carbon dioxide partial pressure in the western North Pacific surface water during the 1982/83 El Niño event. Tellus 39B, 214–227.

Goyet, C, Peltzer, E.T., 1994. Comparison of the August-September 1991 and 1979 surface partial pressure of CO_2 distribution in the equatorial Pacific Ocean near 150°W Marine Chemistry 45, 257–266.

Goyet, C., Millero, F J., O'Sullivan, D.W., Eischeid, G., McCue, S.J, Bellerby, R G.J., 1998. Temporal variations of pCO_2 in surface seawater of the Arabian Sea in 1995. Deep-Sea Research I 45 (4–5), 609–623

Goyet, C., Healy, R., Ryan, J., 2000. Global distribution of total inorganic carbon and total alkalinity below the deepest winter mixed layer depths. Technical report NPD-076. Carbon Dioxide Information and Analysis Center, Oak Ridge National Laboratory, Oak Ridge Tennessee.

Halpern, D., Knox, R., Luther, D., 1988. Observations of 20-day period meridional current oscillations in the upper ocean along the Pacific equator. Journal of Physical Oceanography 18, 1514–1534.

Hénin, C., DuPenhoat, Y., Ioualalen, M., 1998. Observations of sea surface salinity in the western Pacific fresh pool: large-scale changes in 1992–1995 Journal of Geophysical Research 103, 7523–7536.

Inoue, H.Y., 2000. CO_2 exchange between the atmosphere and the ocean. Carbon cycle studies of the Meteorological Research Institute since 1968. In: Handa, N., Tanoue, E., Hama, T. (Eds.), Dynamics and Characterization of Marine Organic Matter. Terra Scientific Publishing, Tokyo, pp. 509–531.

Inoue, H.Y., Sugimura, Y., 1992 Variations and distributions of CO_2 in and over the equatorial Pacific during the period from the 1986/88 El Niño event to the 1988/89 La Niña event. Tellus 44, 1–22.

Inoue, H., Sugimura, Y., Fushimi, K., 1987. PCO_2 and $\delta^{13}C$ in the air and surface sea water in the western North Pacific. Tellus 39, 228–242.

Inoue, H.Y., Matsueda, H., Ishii, M., Fushimi, K., Hirota, M., Asanuma, I., Takasugi, Y., 1995. Long term trend of the partial pressure of carbon dioxide (pCO_2) in surface waters of the western North Pacific, 1984–1993. Tellus 47B, 391–413.

Inoue, H.Y., Ishii, M., Matsueda, H., Ahoyama, M., 1996. Changes in longitudinal distribution of the partial pressure of CO_2 (pCO_2) in the central and western equatorial Pacific, west of 160°W Geophysical Research Letters 23, 1781–1784.

Inoue, H.Y., Ishii, M., Matsueda, H., Saito, S., Aoyama, M., Tokieda, T., Midorikawa, T., Nemoto, K., Kawano, T., Asanuma, I., Ando, K., Yano, T., Murata, A., 2001. Distributions and variations in the partial pressure of CO_2 in surface waters (pCO_2^w) of the central and western equatorial Pacific during the 1997/98 El Niño event. Marine Chemistry 76 (1), 59–75.

Inoue, H.Y., Ishii, M., Matsueda, H., Saito, S., Midorikawa, T., Nemoto, K., 1999. MRI measurements of partial pressure of CO_2 in surface waters of the Pacific during 1968 to 1970: re-evaluation and comparison of data with those of 1980s and 1990s. Tellus 51B, 830–848.

Ishii, M., Inoue, H.Y., 1995. Air–sea exchange of CO_2 in the central and western equatorial Pacific in 1990. Tellus 47B, 447–460.

JMA, 1999. Report of observation for monitoring background marine pollution, Vol 45. Japan Meteorological Agency, Tokyo, pp. 52 (in Japanese with English abstract).

Keeling, C.D., 1993. Surface ocean CO_2. In: Heimman, M. (Ed.), The Global Carbon Cycle, Vol. 15. Global Environmental Change, NATO ASI Series, Series I.

Keeling, C.D., Revelle, R., 1985. Effects of El Niño/Southern Oscillation on the atmospheric content of carbon dioxide Meteoritics 20, 437–450.

Körtzinger, A., Mintrop, L., Wallace, D.W.R., Johnson, K.M., Neill, C., Tilbrook, B., Towler, P., Inoue, H.Y., Ishii, M., Shaffer, G., Torres Saavedra, R.F., Ohtaki, E., Yamashita, E., Poisson, A., Brunet, C., Schauer, B., Goyet, C., Eischeid, G., 2000. The international air–sea intercomparison of fCO_2 systems during the R/V Meteor Cruise 36/1 in the North Atlantic Ocean. Marine Chemistry 72 (2–4), 171–192.

Landry, M.R., Barber, R.T., Bidigare, R.R., Chai, F., Coale, K.H., Dam, H.G., Lewis, M.R., Lindley, S.T., McCarthy, J.J., Roman, M.R., Stoecker, D.K., Verity, P.G., White, J.R., 1997. Iron and grazing constraints on primary production in the central equatorial Pacific: an EqPac synthesis. Limnology and Oceanography 42, 405–418.

Le Borgne, R., Brunet, C., Eldin, G., Radenac, M.-H., Rodier, M., 1995. In: Campagne océanographique FLUPAC Recueil de données, Tome 1. Archives Sciences de la Mer, Océanographie, No. 1, ORSTOM, 337pp.

Le Borgne, R., Barber, R.T., Delcroix, T., Inoue, H.Y., Mackey, D.J., Rodier, M., 2002. Pacific warm pool and divergence: temporal and zonal variations on the equator and their effects on the biological pump. Deep-Sea Research II 49, 2471–2512.

Lee, K., Wanninkhof, R., Takahashi, T., Doney, S., Feely, R.A., 1998. No evidence for large interannual variations in oceanic carbon uptake. Nature 396, 155

Lefevre, N., Dandonneau, Y., 1992. Air–sea CO_2 fluxes in the equatorial Pacific in January–March 1991. Geophysical Research Letters 19 (22), 2223–2226

Lefevre, N., Andrie, C., Dandonneau, Y., Reverdin, G., Rodier, M., 1994. PCO_2, chemical properties, and estimated new production in the equatorial Pacific in January–March 1991. Journal of Geophysical Research 99, 12639–12654.

Le Quéré, C., Orr, J.C., Monfray, P., Aumont, O., Madec, G., 2000. Interannual variability of the oceanic sink of CO_2 from 1979 through 1997. Global Biogeochemical Cycles 14 (4), 1247–1265.

Levitus, S., ConKright, M.E., Reid, J.L., Najjar, R.G., Mantyla, A., 1993. Distribution of nitrate, phosphate and silicate in the world oceans. Progress in Oceanography 31, 245–273.

Lindstrom, E., Lukas, R., Fine, R., Firing, E., Godfrey, S., Meyers, G., Tsuchiya, M., 1987. The Western Equatorial Pacific Ocean Circulation Study. Nature (London) 330, 533–537.

Lukas, R., Lindstrom, E., 1991. The mixed layer of the western equatorial Pacific Ocean. Journal of Geophysical Research 96, 3343–3357.

Luther, D.S., Harrison, D.E., Knox, R., 1983. Zonal winds in the central equatorial Pacific and El Niño. Science 222, 327–330.

Mackey, D.J., Parslow, J., Higgins, H.W., Griffiths, F.B., O'Sullivan, J.E., 1995. Plankton productivity and

biomass in the western equatorial Pacific: biological and physical controls. Deep-Sea Research II 42 (2–3), 499–533.

Mackey, D.J., Parslow, J.S., Griffiths, F.B., Higgins, H.W., Tilbrook, B., 1997. Phytoplankton productivity and the carbon cycle in the western equatorial Pacific under ENSO and non-ENSO conditions. Deep-Sea Research II 44 (9–10), 1951–1978.

Mackey, D.J., Blanchot, J., Higgins, H.W., Neveux, J., 2002. Phytoplankton abundance and community structure in the equatorial Pacific. Deep-Sea Research II 49, 2561–2582.

Madden, R.A., Julian, P.R., 1971. Detection of a 40–50 day oscillation in the zonal wind in the tropical Pacific. Journal of Atmospheric Science 28, 702–708.

Madden, R.A., Julian, P.R., 1972. Description of global-scale circulation cells in the tropics with a 40–50 day period. Journal of Atmospheric Research 29, 1109–1123.

McCarthy, J.J., Garside, C., Nevins, J.L., Barber, R.T., 1996. New production along 140°W in the equatorial Pacific during and after the 1992 El Niño event. Deep-Sea Research II 43 (4–6), 1065–1093.

McPhaden, M.J , 1999. Genesis and evolution of the 1997–98 El Niño. Science 283, 950–954.

Metzl, N., Brès, B., 1996. Mesure en continu de CO_2 dans les eaux de surface. In: Edité par T. Moutin et B. Coste, Campagne Oceanographique OLIPAC, Recueil de données, pp. 217–219.

Metzl, N., Poisson, A., Louanchi, F., Brunet, C., Schauer, B., Brès, B., 1995. Spatio-temporal distributions of air–sea fluxes of CO_2 in the Indian and Antarctic oceans, a first step. Tellus 47B, 56–69.

Metzl, N., Louanchi, F., Poisson, A., 1998. Seasonal and interannual variations of sea surface carbon dioxide in the subtropical Indian Ocean. Marine Chemistry 60, 131–146.

Meyers, D., O'Brien, J.J., 1995. Pacific Ocean influences atmospheric carbon dioxide, EOS Trans. American Geophysical Union 76 (52), 533–537.

Murphy, P.P., Kelly, K.C., Feely, R.A., Gammon, R.H., 1995. Carbon dioxide concentrations in surface water and the atmosphere during 1986–1989 PMEL cruises in the Pacific and Indian Oceans. CDIAC, ORNL/CDIAC-75 NDP-047, 1995.

Murtugudde, R., Signorini, S., Christian, J.R., Busalacchi, A.J., McClain, C.R, Picaut, J., 1999. Ocean color variability in the tropical Indo-Pacific basin observed by SeaWiFS during 1997–1998. Journal of Geophysical Research 104, 18351–18366.

Picaut, J., Ioualalen, M., Menkes, C., Delcroix, T., McPhaden, M.J., 1996. Mechanism of the zonal displacements of the Pacific warm pool: implications for ENSO. Science 274, 1486–1489.

Poisson, A., Metzl, N., Brunet, C., Schauer, B., Brès, B., Ruiz-Pino, D., Louanchi, F., 1993. Variability of sources and sinks of CO_2 and in the Western Indian and Southern Oceans during the year 1991. Journal of Geophysical Research 98 (C12), 22759–22778.

Quay, P., 1997. Was a carbon balance measured in the equatorial Pacific during JGOFS? Deep-Sea Research II 44 (9–10), 1765–1782.

Radenac, M.-H., Rodier, M., 1996. Nitrate and chlorophyll distributions in relation to thermohaline and current structures in the western tropical Pacific during 1985–1989. Deep Sea Research II 43 (4–6), 725–752.

Rayner, P.J., Law, R.M., Dargaville, R., 1999. The relationship between tropical CO_2 fluxes and the El Niño-Southern Oscillation. Geophysical Research Letters 26 (4), 493–496.

Rodier, M., Le Borgne, R., 1997. Export flux of particles at the equator in the western and central Pacific Ocean. Deep-Sea Research II 44, 2085–2113.

Rodier, M., Eldin, G., Le Borgne, R., 2000 The western boundary of the equatorial Pacific upwelling: some consequences of climate variability on hydrological and planktonic properties. Journal of Oceanography 56, 463–471.

Roemmich, D., Morris, M., Young, W.R., Donguy, J.R., 1994. Fresh equatorial jets. Journal of Physical Oceanography 24, 540–558.

Smethie Jr., W.M., Takahashi, T., Chipman, D.W., Ledwell, J.R., 1985. Gas exchange and CO_2 flux in the Atlantic including ^{222}Rn and pCO_2 measurements. Journal of Geophysical Research 90 (C4), 7005–7022.

Stoens, A., Menkes, C., Radenac, M.-H., Dandonneau, Y., Coste, B., Grima, N., Eldin, G., Mémery, L , Navarette, C., Moutin, T., Raimbault, P., 1999. The coupled physical-new production system in the equatorial Pacific Ocean during the 1992–1995 El Niño. Journal of Geophysical Research 104, 3323–3339.

Takahashi, T., Olafsson, J., Goddard, J.G., Chipman, D.W., Sutherland, S C , 1993. Seasonal variation of CO_2 in the high-latitude surface oceans: a comparative study. Global Biogeochemical Cycles 7 (4), 843–878.

Takahashi, T., Feely, R.A., Weiss, R.F., Wanninkhof, R., Chipman, D.W., Sutherland, S.C., Takahashi, T.T., 1997. Global air–sea flux of CO_2: an estimate based on measurements of sea–air pCO_2 difference. Proceedings of the National Academy of Sciences, USA 94, 8292–8299.

Tans, P.P., Fung, I.Y., Takahashi, T., 1990. Observational constraints on the global atmospheric CO_2 budget. Science 247, 1431–1438.

Toggweiler, J.R., Carson, S., 1995. What are upwelling systems contributing to global nutrient and carbon budgets? In: Summerhayes, C., et al. (Ed.), Upwelling the Ocean: Modern Processes and Ancient Records. John Wiley & Sons, Inc., Chichester, England.

Toggweiler, J.R., Dixon, K., Broecker, W.S., 1991. The Peru upwelling and the ventilation of the South Pacific Thermocline. Journal of Geophysical Research 96 (c11), 20467–20497.

Volk, T., 1989. Effect of the equatorial Pacific upwelling on atmospheric CO_2 during the 1982–1983 El Niño. Global Biogeochemical Cycles 3 (3), 267–279.

Wanninkhof, R , 1992. Relationship between gas exchange and wind speed over the ocean. Journal of Geophysical Research 97, 7373–7381.

Wanninkhof, R., Thoning, K., 1993. Measurement of fugacity of CO_2 in surface water using continuous and discrete sampling methods. Marine Chemistry 44 (2–4), 189–205.

Wanninkhof, R., Feely, R.A., Atwood, D.K., Berberian, G.A , Wilson, W D., Murphy, P.P., Lamb, M.F., 1995. Seasonal and lateral variations in carbon chemistry of surface water in the eastern equatorial Pacific during 1992. Deep-Sea Research II 42 (2–3), 387–410.

Wanninkhof, R., Feely, R.A., Chen, H., Cosca, C.E., Murphy, P.P., 1996. Surface water fCO_2 in the eastern equatorial Pacific during the 1992–1993 El Niño. Journal of Geophysical Research 101, 16333–16343

Watson, A.J., Robinson, C., Robinson, J E., Williams, P.J., le, B., Fasham, M.J.R., 1991. Spatial Variability in the sink for atmospheric carbon dioxide in the North Atlantic. Nature 350, 50–53.

Weiss, R.F., Jankhe, R.A., Keeling, C.D., 1982. Seasonal effects of temperature and salinity on the partial pressure of CO_2 in seawater. Nature 300, 511–513.

Weiss, R.F., Van Woy, F.A., Salameh, P.K., 1994. Surface Water and atmospheric carbon dioxide and nitrous oxide observations by shipboard automated gas chromatography: results from expeditions between 1977 and 1990. SIO 92-11. ORNL/CDIAC-59, NDP-044. Carbon Dioxide Information Analysis Center, Oak Ridge National Laboratory, Oak Ridge, Tennessee, 144pp

Winguth, A.M.E., Heimann Kurz, K.D., Maier-Reimer, E., Mikolajewicz, U., Segschneider, J., 1994. ENSO related fluctuations of the marine carbon cycle. Global Biogeochemical Cycles 8, 39–63.

Winn, C.D., Li, Y.-H., Mackenzie, F.T., Karl, D.M., 1998. Rising surface ocean dissolved inorganic carbon at the Hawaii Ocean Time-series site. Marine Chemistry 60 (1/2), 33–47.

Wong, C.S., Chan, Y.-H., Page, J.S., Smith, G.E., Bellegay, R.D., 1993. Changes in equatorial CO_2 flux and new production estimated from CO_2 and nutrient levels in Pacific surface waters during the 1986/87 El Niño. Tellus 45B, 64–79.

Yu, L., Reinecker, M., 1998 Evidence of an extratropical atmospheric influence during the onset of the 1997–98 El Niño. Geophysical Research Letters 25, 3537–3540

Feely R.A., Boutin J., Cosca C.E., Dandonneau Yves, Etcheto J., Inoue H. Y., Ishii M., Le Quéré C., Mackey D.J., McPhaden M., Metzl N., Poisson A., Wanninkhof R. (2002)

Seasonal and interannual variability of CO2 in the equatorial Pacific

In : Le Borgne Robert (ed.), Feely R.A. (ed.), Mackey D.J. (ed.). The equatorial Pacific JGOFS synthesis. *Deep-Sea Research.Part 2 : Topical Studies in Oceanography*, 49 (13-14), p. 2443-2469

ISSN 0967-0645.